DOI: 10.1111/nyas.15180

TECHNICAL REPORT

ANNALS OF THE NEW YORK ACADEMY OF SCIENCES

NYC NPCC4

NPCC4: Tail risk, climate drivers of extreme heat, and new methods for extreme event projections

Luis Ortiz[1] | Christian Braneon[2,3,4] | Radley Horton[4,5] | Daniel Bader[3,6] | Philip Orton[7] | Vivien Gornitz[3] | Bernice Rosenzweig[8] | Timon McPhearson[9,10,11] | Lauren Smalls-Mantey[12] | Hadia Sheerazi[13] | Franco A. Montalto[14] | Mobin Rahimi Golkhandan[14] | Colin Evans[15] | Arthur DeGaetano[15] | Evan Mallen[16] | Latonya Carter[17] | Kathryn McConnell[18] | Talea Mayo[19] | Maya Buchanan[20]

[1]Department of Atmospheric, Oceanic, and Earth Sciences, George Mason University, Fairfax, Virginia, USA

[2]CUNY Institute for Demographic Research (CIDR), City University of New York, New York City, New York, USA

[3]NASA Goddard Institute for Space Studies, New York City, New York, USA

[4]Columbia Climate School, Columbia University, New York City, New York, USA

[5]Lamont-Doherty Earth Observatory, Columbia University, Palisades, New York, USA

[6]Center for Climate Systems Research, Columbia University, New York City, New York, USA

[7]Stevens Institute of Technology, Hoboken, New Jersey, USA

[8]Department of Environmental Science, Sarah Lawrence College, Bronxville, New York, USA

[9]Urban Systems Lab, The New School, New York City, New York, USA

[10]Cary Institute of Ecosystem Studies, Millbrook, New York, USA

[11]Stockholm Resilience Centre, Stockholm University, Stockholm, Sweden

[12]New York City Department of Health and Mental Hygiene, New York City, New York, USA

[13]Rocky Mountain Institute, New York City, New York, USA

[14]Department of Civil, Architectural and Environmental Engineering, Drexel University, Philadelphia, Pennsylvania, USA

[15]Earth and Atmospheric Sciences, Cornell University, Ithaca, New York, USA

[16]Urban Climate Lab, School of City and Regional Planning, Georgia Institute of Technology, Atlanta, Georgia, USA

[17]Department of Geography and Geoinformation Science, George Mason University, Fairfax, Virginia, USA

[18]Department of Sociology, The University of British Columbia, Vancouver, British Columbia, CA

[19]Department of Mathematics, Emory University, Atlanta, Georgia, USA

[20]WSP USA, Portland, Oregon, USA

Correspondence
Luis Ortiz, Atmospheric, Oceanic, and Earth Sciences Department, George Mason University, Fairfax, VA. Email: lortizur@gmu.edu

Christian Braneon, CUNY Institute for Demographic Research at the City University of New York, NASA Goddard Institute for

Abstract

We summarize historic New York City (NYC) climate change trends and provide the latest scientific analyses on projected future changes based on a range of global greenhouse gas emissions scenarios. Building on previous NPCC assessment reports, we describe new methods used to develop the projections of record for sea level rise,

Space Studies, New York City, NY. Email: christian.v.braneon@nasa.gov

Funding information
AXA Research Fund; National Science Foundation, Grant/Award Numbers: 1444755, 1927167, 193493; National Science Foundation Human-Environment and Geographical Sciences (HEGS) and Sociology Programs, Grant/Award Number: 2117405; Eunice Kennedy Shriver National Institute of Child Health and Human Development, Grant/Award Number: P2C HD041020

temperature, and precipitation for NYC, across multiple emissions pathways and analyze the issue of the "hot models" associated with the 6th phase of the Coupled Model Intercomparison Project (CMIP6) and their potential impact on NYC's climate projections. We describe the state of the science on temperature variability within NYC and explain both the large-scale and regional dynamics that lead to extreme heat events, as well as the local physical drivers that lead to inequitable distributions of exposure to extreme heat. We identify three areas of tail risk and potential for its mischaracterization, including the physical processes of extreme events and the effects of a changing climate. Finally, we review opportunities for future research, with a focus on the *hot model problem* and the intersection of spatial resolution of projections with gaps in knowledge in the impacts of the climate signal on intraurban heat and heat exposure.

KEYWORDS
climate justice and equity, climate risk, climate science, extreme events, tail risk

CONTENTS

1 | CHAPTER SUMMARY

This chapter summarizes historic New York City (NYC) climate change trends and provides the latest state-of-the-art science information on potential future changes based on a range of global greenhouse gas (GHG) emissions scenarios. This chapter further describes the drivers and consequences of climate change in NYC related to sea level rise (SLR), extreme heat, and precipitation. Projections of annual averages, the frequency of extreme temperatures, and precipitation are presented, refining methods used in previous New York City Panel on Climate Change (NPCC) reports.

1.1 | Key messages

Key Message 1: NPCC4 analysis of the impact of "hot models" on the 6th phase of the Coupled Model Intercomparison Project (CMIP6) ensemble found no statistically significant difference between the temperature and precipitation projections of record and alternative projections that do not include models with equilibrium climate sensitivity (ECS) outside the expected range. The CMIP6 climate model ensemble used to create the temperature and precipitation projections of record contains three models that display higher-than-expected sensitivity of temperatures to GHGs. These so-called "hot models" lead to higher global mean temperatures. However, the impact of high climate sensitivity appears small with our approach to developing local projections for NYC. Nevertheless, more research is needed to better understand (1) the impact of the high climate sensitivity on the representation of key large-scale climate processes, (2) the model physics leading to high sensitivity in the first place, and (3) the constraints on the planet's ECS.

Key Message 2: The high tail end of sea level rise (SLR) will be governed by the future stability of the West Antarctic Ice Sheet (WAIS) and Greenland ice sheets throughout the 21st century and beyond. If all marine-based ice melted, the WAIS could contribute ~3m and the Greenland Ice Sheet ~7 m of SLR potential. Troubling signs of ice shelf thinning and ocean warming around WAIS and an approaching temperature tipping point over Greenland raise the possibility of faster and higher SLR than projected by most climate models, increasing the risks associated with coastal flooding. Additional research is needed to gain a better understanding of all the processes governing ice sheet behavior with rising temperatures. Stakeholders concerned with long-term planning need to examine plausible scenarios at the extreme upper tail of the SLR distribution.

Key Message 3: While the occurrence of extreme heat events in NYC is governed in great part by climatic events taking place at large spatial scales, local urbanization patterns play a key role in the spatial distribution of temperatures within the city. These local patterns, which include a range of factors like distribution of green spaces and urban geometry, play the most significant role in the generation of physical process that lead to the urban heat island (UHI). Moreover, extreme heat events exacerbate intraurban excess temperatures, increasing deadly heat exposure for populations without access to adaptive measures and cooling infrastructure (e.g., cooling centers, tree shade). Future work is needed to assess the impact of a warming climate on intraurban heat variability in order to quantify the effect of climate change on spatial inequities of heat exposure.

2 | INTRODUCTION

While every NPCC assessment report has included a chapter on the state of climate science and projections for NYC, this chapter includes a strengthened emphasis on the equity implications of climate change adaptation.[1,2] In addition, this chapter addresses emerging issues related to higher-than-expected ECS in several ensemble members from the CMIP6, which simulate higher-than-expected global mean temperatures. Finally, the chapter describes the changing tail and compound risks associated with climate change.

2.1 | Chapter Scope and Context

Anthropogenic climate change is fundamentally linked to the rapid increase in GHG emissions propelled by the Industrial Revolution and the European colonial systems that enabled it. "Raw materials from colonies across the British Empire fueled the Industrial Revolution,"[3] land dispossession and forced migration facilitated colonial expansion, and chattel slavery provided unpaid labor to build the British colonies as well as the new American nation.[1,5–8] In addition, the "political arithmetic" of global trade prompted extreme extraction from the New York metropolitan region's biodiversity into the Atlantic world trading system.[9] Consequently, humanity's climate crisis has its roots in land dispossession, forced migration, as well as human and natural resource extraction orchestrated by European colonial powers.[10–11] Furthermore, the tremendous variability in vulnerability to climate change (among and within regions) is driven by "patterns of intersecting socio-economic development, unsustainable ocean and land use, inequity, and marginalization" as well as "historical and ongoing patterns of inequity such as colonialism" and structural racism (e.g., Home Owners Loan Corporation redlining in NYC's five boroughs).[12–17]

[1] The U.S. share of global GHG emissions is currently around 15%.[4]

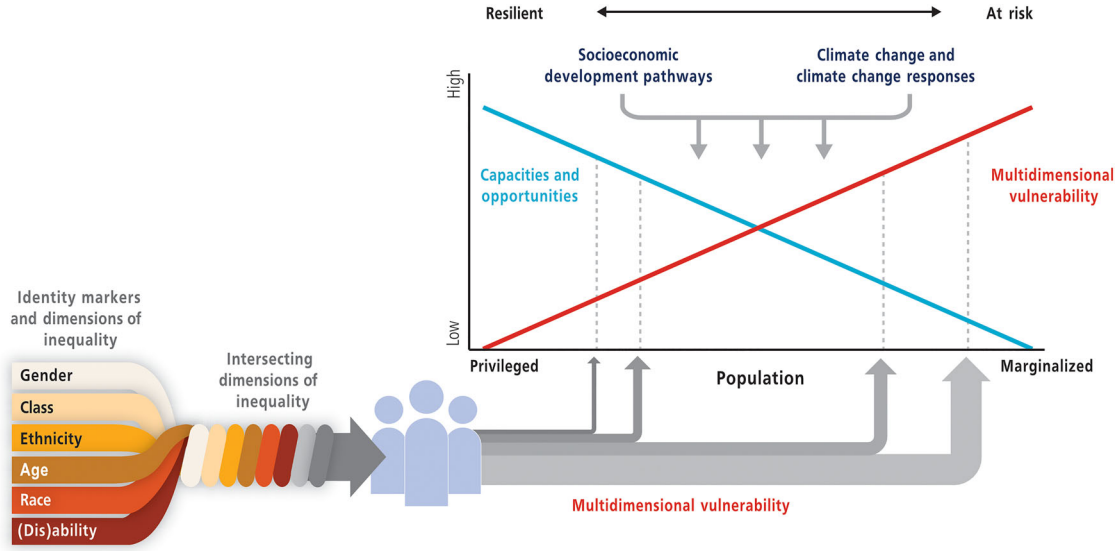

FIGURE 1 Schematic depicting the relationship between marginalization, vulnerability, and resilience. *Source*: Field et al.[18]

Vulnerability to climate hazards and stressors (Figure 1)[18] is unequally distributed across NYC as "high levels of social vulnerability are consistently found in areas with lower incomes," aging populations, and higher proportions of Black and Latinx/Hispanic residents.[2] For example, NYC is among urban hotspots in the country where ambient temperatures can be 5–20° Fahrenheit hotter in neighborhoods with low-income households and more residents of color.[19] NYC also has the largest number of affordable housing units exposed to extreme water levels in the country.[20]

NYC Local Law 42 (LL42) (2012)[21] mandates that NPCC meet at least twice a year for the purpose of (i) reviewing the most recent scientific data related to climate change and its potential impacts on the city's communities, vulnerable populations, and public health[2] as well as the city's natural systems, critical infrastructure, buildings and economy; and (ii) advising municipal staff (e.g., the Mayor's Office of Climate and Environmental Justice) as well as the NYC Climate Change Adaptation Task Force. Further, the NPCC[3] is mandated by LL42 to make recommendations regarding (i) the near-, intermediate-, and long-term quantitative and qualitative climate projections (i.e., "projections of record") for the City of New York; and (ii) a framework for stakeholders to incorporate climate projections into their planning processes.[22]

In 2024, the NPCC published a brief assessment report that aimed to mirror its 2013 report (see Rosenzweig et al.).[23] It establishes new SLR projections of record for NYC and introduces interim climate projections associated with temperature and precipitation. Further, the climate science synthesis focused on SLR that is presented by NPCC4 in "NPCC4: New York City climate risk information 2022–observations and projections."[24] addresses recommendations from NPCC3 to (a) "monitor trends in sea level rise and in the processes contributing to sea level rise in the New York metropolitan region," (b) "study trajectories of potential sea level rise that continue after 2100 in light of the sea level rise commitment on longer timescales," and (c) "examine the consequences of long-term sea level rise scenarios on coastal flooding, including those stemming from low-probability, high-end scenarios."[25]

This chapter presents the finalized projections of record[4] associated with temperature and precipitation. These projections use new methods that derive expected changes in NYC's temperature and precipitation from global climate models (GCMs), both in terms of average conditions as well as climate extremes. The projections use the newest generation of climate models from CMIP6, which include significant advances in the representation of the processes that form the climate system and the impacts of anthropogenic emissions. New methods for downscaling GCM outputs are introduced which account for changes to not only the mean state of local climate but also in the variability of temperature and precipitation.

The chapter also describes the potential impacts of climate change on intraurban heat variability. While the chapter does not update the projections of NPCC3 that mapped temperatures at the neighborhood scale for select future periods of time,[26] it describes the local and global drivers of extreme heat in the city. Moreover, new projections of compound heat and humidity are presented. A new section also describes

[2] Vulnerable populations are defined here as persons or communities at increased risk of harm as a direct or indirect consequence of climate change based on one or more of the following risk factors: (i) proximity to disproportionally impacted areas; (ii) age, including senior citizen or minor status; (iii) income level; (iv) disability; (v) chronic or mental illness; and (vi) language. Public health is defined here as impacts on physical health, mental health, and social well-being, and public or private services that treat and prevent disease, prolong life, and promote health.

[3] The Panel is currently led by a team of four co-chairs who possess a broad spectrum of disciplinary expertise, including climate science, demography, civil and environmental engineering, geography, vulnerability analysis, global change, architecture, and urban planning. Both the full NPCC and its leadership team were selected to ensure a diversity of backgrounds, research disciplines, and fields of technical practice.

[4] Based on climate analyses, regional and global trends, and a review of scientific literature, NPCC confirms which climate projections of temperature, precipitation, sea level rise, and coastal flooding (i.e. projections of record) are most appropriate for use in resiliency planning for the city and region.

growing evidence of global climate change leading to stronger UHIs as well as physical interactions that may exacerbate NYC's UHI.

2.2 | Chapter Organization

This chapter contains three sections that describe changing climate risks in NYC. Section 3 builds on previous NPCC assessment reports by describing the latest climate science and data, while describing new methods used to develop the projections of record for SLR, temperature, and precipitation for use by the City. This section also describes the approach followed by NPCC4 for using projections across multiple emissions pathways. Finally, Section 3 also discusses the issue of the "hot models" associated with CMIP6 and their potential impact on NYC's climate projections. Section 4 describes the state of the science on temperature variability within the city. This section explains both the large-scale and regional dynamics that lead to extreme heat events, as well as the local physical drivers that lead to inequitable distributions of exposure to extreme heat. Section 5 describes the physical processes and the impact of a changing climate on *tail risks* and extreme events. Finally, Section 6 reviews opportunities for future research, with a focus on the *hot model problem* and the intersection of spatial resolution of projections with gaps in knowledge in the impacts of the climate signal on intraurban heat and heat exposure.

3 | SUSTAINED ASSESSMENT AND CMIP6

This report follows prior NPCC assessments that developed climate projections for NYC. Presented here is a summary of the methods and how the key components of the projections have changed over time. Braneon et al.[24] and the New York State Climate Impacts Assessment (NYSCIA)[27] provide a more detailed description of the analytic methodology. The NYSCIA contains a detailed breakdown of the differences in each element of the projections (e.g., baseline period, number of models used, emissions scenarios).

3.1 | Identifying the differences and updates in the climate projections

Changes in the projections in this NPCC4 report include (1) the use of new emissions scenarios and GCMs, (2) updated historical baseline period and future time slices for projections, and (3) new methods for projections of quantitative extreme events and SLR.

3.1.1 | Emissions scenarios and global climate models

The newest climate science available is associated with CMIP6; its shared socio-economic pathways (SSPs) are part of a new scenario framework,[28,29] established by the climate change research community to facilitate the integrated analysis of future climate impacts, vulnerabilities, adaptation, and mitigation. The updated climate projections for NYC utilize data (both monthly and daily) from the CMIP6 ensemble of global climate models (GCMs). For a specific description of the methods used, refer to Braneon et al.[24]

CMIP6 GCMs have, in general, a higher spatial resolution than CMIP5 (the previous iteration of models utilized by the IPCC); grid box sizes for many models are on the order of approximately 70 miles by 70 miles horizontally, whereas a common resolution for CMIP5 was approximately 140 miles by 140 miles. CMIP6 models also feature more advanced characterization of key system components, such as stratospheric chemistry, and more dynamic coupling across system components. The climate sensitivity—a measure of how sensitive global average temperatures are to changes in GHG concentrations—is higher in approximately one-fourth of CMIP6 models than in CMIP5 and earlier CMIP generations.[30] In addition to presenting projections for NYC based on CMIP6, this chapter also examines the potential impact of these so-called hot models.

3.1.2 | Historical base period and future time slices

The historical baseline periods for the climate projections are updated for NPCC4. Projections of temperature are expressed relative to a baseline period of 1981–2010 for temperature and precipitation, while the baseline period is 1995–2014 for SLR. In addition, projections are now provided for each decade from the 2030s through the 2080s (see Braneon et al.[24] for more details). The methods still use a 30-year average for the time periods (10-year average for SLR) to reduce the noise of year-to-year variability while the climate change signal remains.

3.1.3 | New methods for extreme events and sea level rise

For the projections in NPCC4, new methodologies are used for quantitative extreme events and SLR. Full details of these methods can be found in Braneon et al.;[24] however, this section identifies some of the key updates.

In NPCC4, quantile mapping is used to combine the daily outputs from the GCMs with historical climate data to develop future climate projections that include daily extremes like hot days, defined as days with maximum temperature above 90°F and days with heavy rainfall, defined as days with at least 1-inch total precipitation. Quantile mapping represents an advance from prior NPCC work, which used the delta method based on monthly rather than daily data from GCMs. Whereas the delta method largely retains the distribution of temperatures from the historical observed data—only adding a mean, or delta, uniformly to the historical data, quantile mapping of daily data retains changes in the distribution of temperatures with climate change, as simulated by GCMs. For example, if a model has its top 1% of hottest days warming more than other days, quantile mapping will lead to

projections with larger increases in hot day frequency and intensity than would be generated by the delta method.[31]

The downscaling technique used in this work is one of many used in climate research, and while all are generally considered to render value added projections (by addressing GCM biases and adding finer spatial resolution), the methods do not produce identical results. The downscaling technique used here should not be considered inherently superior to other possible downscaling choices.

The development of a comprehensive approach to SLR in the latest IPCC report (AR6) offered the opportunity to rely on methods and data generated by the IPCC rather than recreating data already available. For NYC, outputs are taken directly from the IPCC data set for the Battery for three scenarios: SSP2-4.5-medium confidence, SSP5-8.5-medium confidence, and SSP5-8.5-low confidence.[32] Because these data are available for years at the start of each decade (e.g., 2050), we interpolated the values to the middle year (e.g., 2055) of the decade, to align with the decadal time periods (e.g., the 2050s) previously used for NPCC SLR projections. SLR projections are computed for all decades from the 2030s to the 2090s and then 2100 and 2150.

3.1.4 | Additional methodological changes and advances

The observed rate of mean SLR of 4.3 ± 1.08 mm/year (1992–2021) at the Battery in NYC[33,34] remains higher that of the observed rate of global mean sea level rise (GMSLR) of 3.3 [2.8–2.2] mm/year (1993–2018).[35] This higher relative, or local rate of sea level rise (RSLR) derives from a combination of glacial isostatic adjustment-related subsidence, enhanced thermal expansion, and increasing distant land ice mass losses (see also [24]; Section 4.1.1). New hotspots of highly localized land uplift and subsidence in NYC that cause variations in RSLR have been recently identified by interferometric synthetic aperture radar and other satellite data.[36] Most of these hotspots are situated on land fill or on heavily modified ground. The very localized variations in RSLR may produce highly differential coastal flood risk across the city. In addition, there is some evidence that Atlantic Meridional Overturning Circulation (AMOC) weakening in the future could lead to higher RSLR along much of the East Coast and increase the likelihood of higher coastal flooding.[37,38] Moreover, the AMOC plays a role in a "domino effect" of tipping points, which may add uncertainty to its role in RSLR[39] and other changes throughout the climate system.

SLR and coastal flooding pose growing risks to the population and major economic assets along and beyond NYC's waterfront. Rising sea level is leading to an increased frequency of coastal flooding in NYC and elsewhere in the United States (e.g., Sweet et al.[40]) Future SLR will exacerbate high tide flooding as well as the destruction caused by storm surges.[41]

While the ambiguity associated with ice-sheet instability limited the ability of NPCC3 (and earlier Panels) to generate quantitative sea level projections of record[32,43–45] that explicitly account for this, NPCC4 utilizes SLR projections from the National Aeronautics and Space Administration (NASA) Sea Level Projection Tool[35,42,46] to present a broad range of plausible outcomes that explicitly account for ice sheet processes,[5 47,48] that are deeply uncertain.[24,49] The tool allows users to view both global and regional sea level projections from 2020 to 2150, along with how these projections differ depending on future scenario or warming level (see Figure 2 from NASA[42]).

TABLE 1 Difference in ensemble means for the 2080s for temperature and precipitation metrics.

Metric	Decade	Difference in Means
Days/year > = 90°F	2080s	4.12
Days/year > = 95°F	2080s	3.43
Days/year > = 100°F	2080s	2.65
Days/year < = 32°F	2080s	−4.64
Days/year > = 1 inch	2080s	0.24
Days/year > = 2 inches	2080s	0.08
Days/year > = 4 inches	2080s	0.03

Note: Kolmogorov–Smirnov (KS) tests comparing the 32-member ensemble (16 GCMs × 2 scenarios) of model mean projections (i.e., mean of 30 years of annual projections) for the 2080s with a 26-member ensemble (13 GCMs × 2 scenarios) that excludes GCMs with TCR values greater than 2.2°C. No statistically significant differences are found for any metric at the 0.01 level.

While the SLR projections available from the NASA Sea Level Projection Tool for NYC are consistent with the assessment of ECS described in IPCC's Sixth Assessment Report (AR6) (see Box 9.3 and Sections 9.6.3 and 9.7 in Fox-Kemper et al.[35]), some members of the climate science community (e.g., Hausfather et al.[50]) have begun presenting different approaches (e.g., model culling, or rejecting some models' projections) for projecting local temperature and precipitation changes that explicitly address the fact that some GCMs' transient warming lies outside the bounds of the IPCC AR6 assessed "likely" range of ECS or transient climate response (TCR) (Table 1 in Rypdal et al.[51] shows a TCR span of 1.3–3.0°C in the CMIP6 experiments). A consequential aspect of the model culling approach is that "rejecting models is akin to applying a binary weighting scheme to the CMIP6 ensemble, with zero weight applied to the culled models, and model democracy" (e.g., equal weighting) for the remaining ensemble members.[52] As model culling (or unequal weighting) results in eliminating (or significantly reducing) consideration of the information provided by a significant portion of the model ensemble, NPCC4 has elected to conduct data-driven analyses to understand if the so-called "hot model" problem[50] has a statistically significant impact on the bias-corrected temperature and precipitation projections presented in Braneon et al.[24,52,53]

According to J.R. Lanzante, "In climate science, one of the most fundamental pursuits is determination of the significance of differences between two states or sets of conditions."[54] Multiple statistical tests were conducted with the ensemble of GCM means that is used to

[5] To indicate the potential impact of deeply uncertain ice sheet processes, about which there is currently a low level of agreement and limited evidence, low confidence projections are also provided for SSP1-2.6 and SSP5-8.5. For both the Greenland and Antarctic ice sheets, the low confidence projections integrate information from the Structured Expert Judgement study of Bamber et al.[47] For the Antarctic ice sheet, the low confidence projections, projections also incorporate results from a simulation study that incorporates Marine Ice Cliff Instability.[48]

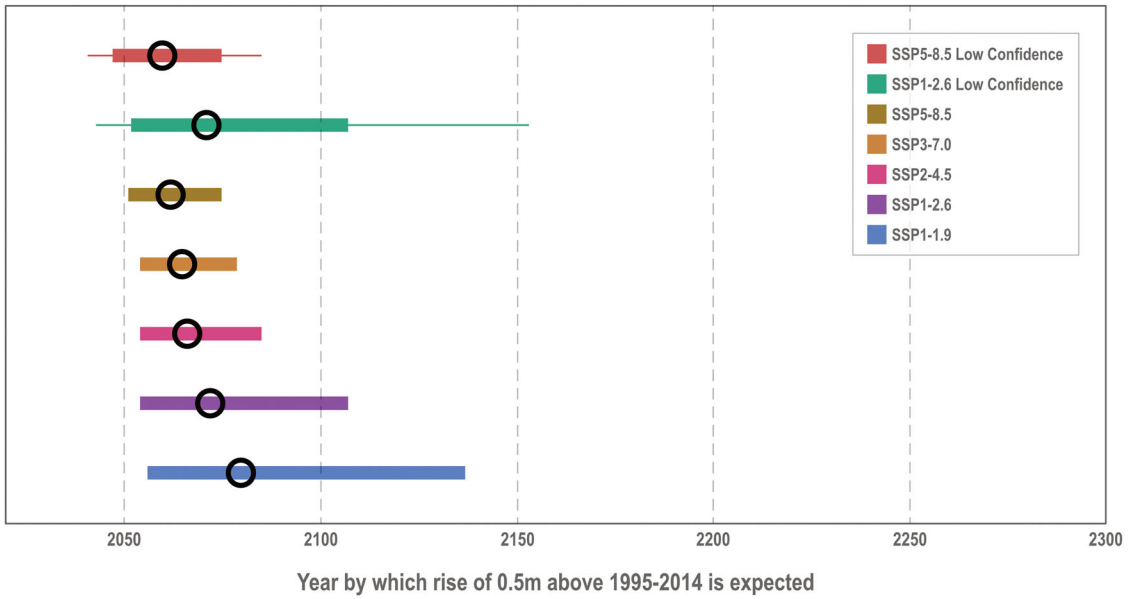

FIGURE 2 Projected timing of selected sea level rise milestone under different scenarios at The Battery in New York City. Thick bars show 17th–83rd percentile ranges, and black circles show median value. Thin bars also show 5th–95th percentile ranges for SSP1-2.6 Low Confidence and SSP5-8.5 Low Confidence scenarios that indicate the potential impact of deeply uncertain ice sheet processes. *Source*: National Aeronautics and Space Administration.[42]

develop the temperature and precipitation projections found in Braneon et al.[24] Kolmogorov–Smirnov tests results reveal that there is no statistically significant difference at the significance level of 0.01 for any of the metric distributions when the three GCMs with TCR values greater than 2.2°C are removed (see Table 1 for 2080s results). NPCC4 affirms the temperature and precipitation projections presented here (and also in Section 6.4 of Braneon et al. [24]) as projections of record for the City of New York. Appendix A shows boxplots comparing 960-member ensembles (16 GCMs × 2 scenarios × 30 years) of annual projections with 780-member ensembles (13 GCMs × 2 scenarios × 30 years) that exclude GCMs with TCR values greater than 2.2°C (Figures A1–A3).

3.1.5 | Temperature trends and projections

Annual average air temperatures, as measured by long-term ground observations in the Global Historical Climatological Network daily (GHCN-daily),[55] have increased at stations across the NYC metropolitan area over the last 70 years. Although the data records' length varies between stations, the warming rates are similar. During their overlapping period of observations (1949–2022), annual mean temperatures have increased at rates between 0.24°F and 0.41°F per decade (Figure 3). This increasing trend can be observed across the entire observation record of each station, with Central Park temperatures growing at a pace of 0.28°F per decade since 1870. Overall, however, temperature changes are not linear in time, and may exhibit different decadal trends across long observation time spans. For example, annual mean temperatures have increased at a faster rate since

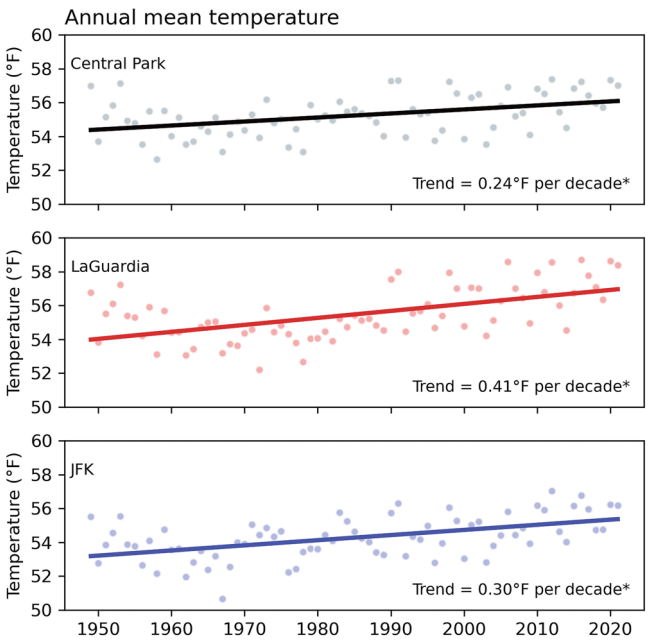

FIGURE 3 Annual mean temperature recorded at Central Park, LaGuardia Airport, and JFK Airport (1949–2022). Solid line represents linear trend. *Trend is significant at the 99% confidence level tested with a nonparametric Spearman correlation. *Source*: Global Historical Climatology Network-daily.

1995, with observations at Central Park, LaGuardia, and JFK stations reaching 0.64°F, 0.74°F, and 0.71°F per decade.

Both daily minimum and maximum temperatures have increased throughout this period (Figure 4). In general, nighttime minimum

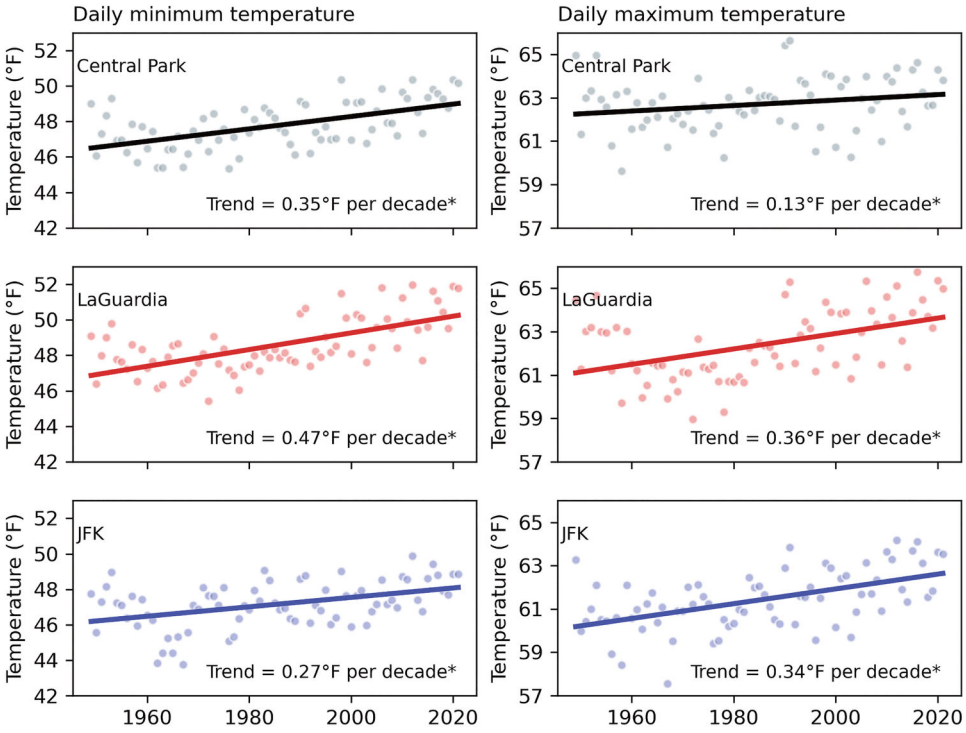

FIGURE 4 Annual daily minimum (left column) and maximum (right column) temperature recorded at Central Park, LaGuardia, and JFK Airports (1949–2022). Solid line represents linear trend. *Trend is significant at the 95% confidence level tested with a nonparametric Spearman correlation. *Source*: Global Historical Climatology Network-daily.

temperatures have increased at faster rates than daytime maximum, except at John F Kennedy (JFK) Airport. As in annual average temperatures, similar trends are observed in both daily minima and maxima when the records are extended beyond their temporal overlap, with Central Park station daily minimum and maximum growing by 0.26°F and 0.31°F per decade since the first observations in 1870.

Climate change is extremely likely to bring warmer temperatures to the New York metropolitan region. As in annual mean temperatures, daily minimum and maximum trends have increased at a faster rate more recently. Since 1995, daily minimum temperatures have increased at rates of 0.73°F, 0.74°F, and 0.68°F per decade in the Central Park, LaGuardia, and JFK stations, respectively. Likewise, daily maxima have increased at a rate of 0.55°F, 0.74°F, and 0.74°F per decade during this period.

GCMs project a mean annual average temperature increase between 2.7 and 3.9°F by the 2030s, 4.0 and 6.0°F by the 2050s, and 5.6 and 9.8°F by the 2080s relative to a baseline period of 1981–2010. The total number of hot days and nights in NYC is projected to increase between 15 and 52 days by midcentury. The frequency of heat waves is expected to increase by a factor of 2–4 times the current baseline, with their average duration increasing by up to 50% by the 2050s. By the 2080s, the projected number of days per year with maximum temperatures at or above 82°F (which occur on average 69 days per year in the current climate) nearly doubles. By the 2080s, the upper end of projected number of days per year with minimum temperatures at or above 80°F (which occur on average about 1 day per year in the current climate) increases 10-fold.

3.1.6 | Heat index projections

In order to maintain biological function, humans must keep a body temperature of close to 37°C (98.6°F). However, humans gain heat through a variety of mechanisms such as metabolic activity and from interactions with the environment. In order to maintain body temperatures near 37°C, the human body sheds heat via convection, evaporation of surface sweat, and respiration. Of these, evaporation is the most important as it accounts for close to 75% of heat dissipation.[56] However, evaporation of surface skin sweat is dependent on the properties of moist ambient air. As ambient air around a person becomes saturated with moisture, evaporation becomes more difficult, leading to reduced heat dissipation. This reduced cooling capacity can be particularly dangerous during periods of extreme heat, when humans are most reliant on evaporation for shedding heat.

Although there are several methods to quantify the impact of combined temperatures and humidity on human wellbeing, the United States National Weather Service (US NWS) relies on the heat index as defined by Steadman[57] and codified into an equation by Rothfusz.[58,6]

[6] A recent study by Lu and Romps[59] found that the NWS formula used to calculate heat index may lead to negative biases when applied to future climate scenarios. This paper was not available at the time when the climate projections were updated.

TABLE 2 Projections of heat index days per year for 30-year periods centered around the 2040s, 2050s, 2060s, 2070s, and 2080s.

	Baseline period (1981–2010)	10th	25th	50th	75th	90th
2030s						
Days with HI > 85°F	38	57	61	69	74	84
Days with HI > 95°F	6	17	18	23	29	37
2040s						
Days with HI > 85°F	38	60	67	77	84	92
Days with HI > 95°F	6	19	23	29	36	44
2050s						
Days with HI > 85°F	38	68	74	83	93	102
Days with HI > 95°F	6	23	30	37	46	57
2060s						
Days with HI > 85°F	38	72	81	92	100	112
Days with HI > 95°F	6	27	33	46	54	70
2070s						
Days with HI > 85°F	38	77	86	97	109	121
Days with HI > 95°F	6	31	37	50	65	82
2080s						
Days with HI > 85°F	38	81	89	101	118	132
Days with HI > 95°F	6	34	39	55	77	97

Table 2 shows the baseline (1981–2010) and projected changes to the occurrence of extreme heat index days throughout the 21st century. In the recent historical record, NYC experiences, on average, 38 and 6 days with a heat index above 85°F and 95°F, respectively. These heat index thresholds are labeled by the US NWS as periods where *caution* and *extreme caution* are warranted. By mid-century (2050s), the number of heat days with a heat index larger than 95°F is projected to increase sixfold to 37 (the 50th percentile value of the model-based projections). Meanwhile, end-of-century days with a heat index above 95°F increase close to a factor of 9 (50th percentile).

These results build on work presented in NPCC3[26] by introducing a full set of projections of record of compound humid heat occurrence for the first time in NPCC. These projections leverage subdaily data from CMIP6, the quantile mapping method used for the other projections on model air temperatures and relative humidity estimates to present data consistent with projections of temperature, precipitation, and their extremes.

3.1.7 | Precipitation trends and projections

Annual precipitation has increased since 1959, as recorded across all three long-term weather stations in NYC. The Central Park and LaGuardia stations exhibit similar statistically significant positive trends of 1.61 and 1.35 inches more rain per decade. Meanwhile, rainfall at JFK airport station exhibits a slightly lower and not statistically significant trend of 0.93 inches more rain per decade (Figure 5).

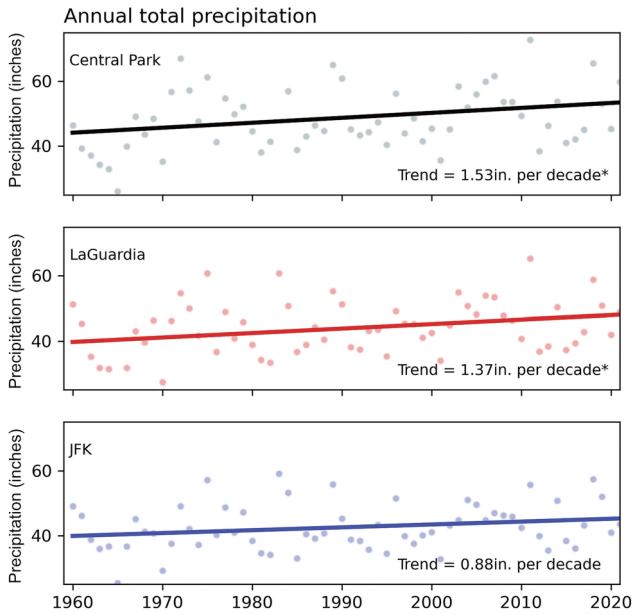

FIGURE 5 Annual total precipitation recorded at the Central Park, LaGuardia, and JFK stations for their overlapping period of observations (1960–2022). Solid line represents linear trend. *Trend is significant at the 95% confidence level. *Source*: Global Historical Climatology Network-daily.

Total annual precipitation will likely increase, although precipitation projections are less certain than temperature projections. Mean annual precipitation is projected to increase by approximately 2–7% by the

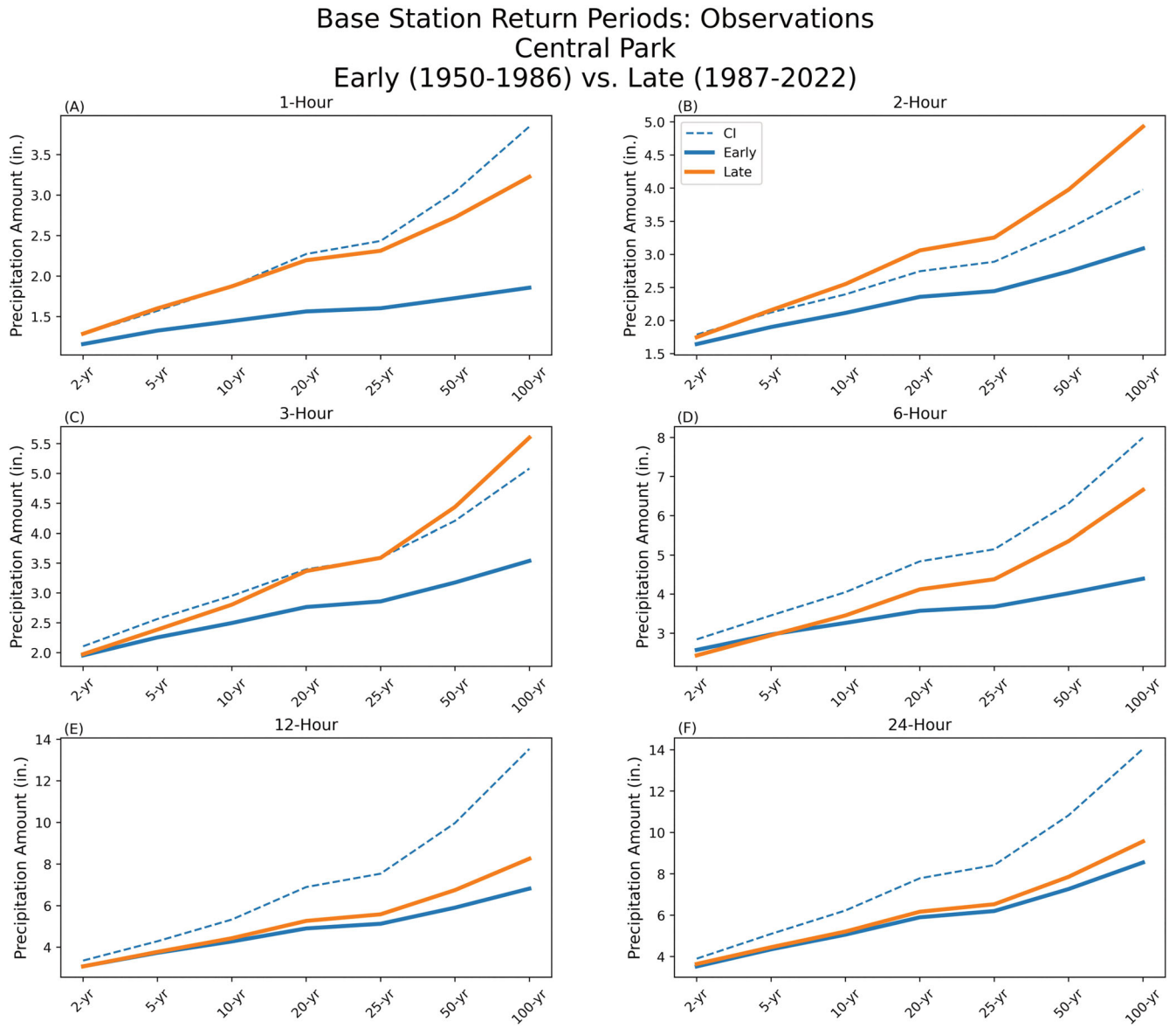

FIGURE 6 Intensity-duration-frequency chart created from two sets of partial duration series (PDS): early (1950–1986, blue) and late (1987–2022, orange) for differing hourly durations (Panels A–F) and recurrence intervals (x-axis). The upper bound of the 90% confidence interval based solely on the 1955–2022 period of record (POR) is plotted in black. *Source*: NCEI Hourly Precipitation Dataset and Local Climatological Dataset.

2030s, 4–11% by the 2050s, and 7–17% by the 2080s relative to a baseline period of 1981–2010. The frequency of extreme precipitation days is projected to increase, with approximately one and a half times more events per year possible by the 2080s compared to the current climate (i.e., compared to the 1981–2010 baseline period).

3.1.8 | New analyses of historical trends and future projections for subdaily precipitation

Along with changes in annual precipitation, climate change will impact patterns of precipitation at subdaily time scales with implications for flooding, harbor water quality, as well as the design and maintenance of building systems and infrastructure. To evaluate historic trends in subdaily precipitation, a 68-year study of historical precipitation was conducted using hourly precipitation data from The NCEI Hourly Precipitation Dataset (HPCP; 1955–2013)[60] and Local Climatological Dataset (LCD; ID NCEI DSI 3505; NCEI 2005; 2014–2022).[61] The analysis included three NYC metropolitan area gauges (Central Park, LaGuardia Airport, and Newark Airport), with JFK Airport excluded due to long periods of missing hourly data.

During this period record, it should be noted that the observing technology in use transitioned. Unshielded Universal (or Freiz) weighing rain gauges were in use during the earliest part of each station's

TABLE 3 Precipitation trends (1955–2022).

	Newark Airport	Central Park	LaGuardia Airport
Annual accumulated precipitation	**Increasing** *	**Increasing** *	**Increasing** *
Annual number of events			
Peak hourly intensity	**Increasing** *	**Increasing** *	**Increasing** *
Frequency of long-term 95th percentile peak hourly intensity exceedances	**Increasing** *	**Increasing** *	**Increasing** *
Frequency of long-term 99th percentile peak hourly intensity exceedances	**Increasing** *		
Event total precipitation accumulation	**Increasing** *		**Increasing** *
Frequency of long-term 95th percentile event total precipitation accumulation exceedances	**Increasing** *	**Increasing** *	
Frequency of long-term 99th percentile event total precipitation accumulation exceedances			
Event duration		**Decreasing** *	**Decreasing** *
Frequency of long-term 95th percentile event duration exceedances			
Frequency of long-term 99th percentile event duration exceedances			
Average hourly intensity	**Increasing** *	**Increasing** *	**Increasing** *
Frequency of long-term 95th percentile average hourly intensity exceedances	**Increasing** *	**Increasing** *	**Increasing** *
Frequency of long-term 99th percentile average hourly intensity exceedances	**Increasing** *	**Increasing** *	

Note: Intensity-duration-frequency curves calculated based on observations from 1955 to 1986 and 1987 to 2022. The recent period values are statistically different from the earlier period, especially at the longer recurrence intervals.
*Trend is significant at the $p < 0.05$ level.
Source: NCEI Hourly Precipitation Dataset and Local Climatological Dataset

record. A tipping-bucket type rain gauge was used at Central Park from 2000 to 2004, at LaGuardia from 1996 to 2004, and at Newark from 2000 to 2005. These transitioned to an NWS all-weather precipitation accumulation gauge in the later part of the record. Wind shielding was added to the gauge at LaGuardia in 2010 and Newark in 2019. It is likely that rainfall measured by the tipping bucket gauges was underestimated, especially when intensity was high. The addition of wind shields likely resulted in a more accurate rainfall measurement. Although these potential biases are an artifact of the entire U.S. national hourly precipitation record, established methods to adjust for these discontinuities are not available.

For these analyses, discrete events were defined by at least a 4-h period without rainfall[62,63] and characterized in terms of the peak hourly intensity observed during the event, the event total accumulation, the event duration, and the average intensity (defined as event total accumulation/duration). The number of events that occurred for each year and each gauge were computed and extreme precipitation events, defined as the number of exceedances of the 95th and 99th percentile values in the full record, were identified. The nonparametric Mann–Kendall test was employed.[64] This test was used to identify statistically significant upward and downward trends using a *p*-value threshold of 0.05. The results from these analyses are summarized in Table 3. Significant increasing trends in the 95th percentile peak hourly intensity and event total intensity were observed at all three sites.

Urban stormwater and other critical infrastructure systems are designed to withstand a defined intensity and duration of rainfall, known as the design storm. For any given rain event, the intensity of rainfall (defined as rainfall depth over a given duration) is associated with an annual probability of occurrence, usually described by its reciprocal recurrence interval. Accurate representation of the probability of rainfall intensity is thus critical for stormwater management and flood resilience planning and design. This information is presented in site-specific intensity-duration-frequency (IDF) curves, developed based on frequency analysis of historic rainfall at specific locations and under the assumption of stationarity—the idea that natural systems fluctuate within an envelope of variability that is unchanging with time.[65] With projections of amplified precipitation intensity through the 21st century due to global climate change,[66–68] the appropriateness of this approach to urban drainage design has recently been called into question.[69]

Two sets of Partial Duration Series (PDS; 1955–1986 and 1987–2022) were constructed separately using hourly precipitation data from the sources described above. For each PDS in the array, IDF

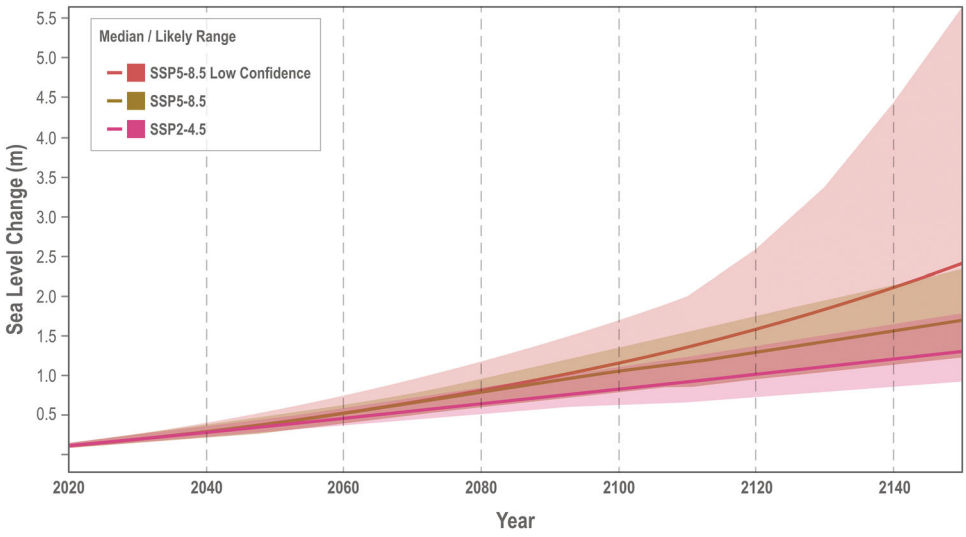

FIGURE 7 Projected sea level rise under different scenarios at The Battery in New York City. Median values for three scenarios are shown with solid lines and shaded regions show the 17th–83rd percentile ranges presented in the IPCC Sixth Assessment Report. Projections are relative to a 1995–2014 baseline. *Source*: National Aeronautics and Space Administration.[42]

curves (Figure 6) describing rainfall amounts corresponding to annual recurrence probabilities of 50%, 20%, 10%, 4%, 2%, and 1% (i.e., 2-, 5-, 10- 25-, 50-, and 100-year storms) were computed by simulating the methodology used in NOAA Atlas 14.[70] As shown in Figure 6, changes between the 1955–1986 and 1987–2022 IDF curves vary with rain event duration and recurrence probability, with substantially greater changes observed for the 1–12 h events at recurrence intervals greater than 25 years. For example, at the Central Park weather station (Figure 6), in the 50-year recurrence interval the change in the 1-h duration is 40%, while for the 24-h duration rain event, it is only 15%.

3.1.9 | Sea level rise projections

SLR in NYC is projected to continue to exceed the global average and is very likely to accelerate as the century progresses. A recent study based on statistics and oceanographic data warns of a potential collapse of the AMOC, an important branch of the global ocean circulation system, as early as the 2050s under current GHG emissions.[71] Most experts only anticipate a future slowing of the AMOC as opposed to a complete collapse;[72] a weakening of the AMOC could lead to increased thermal expansion, and redistribution of ocean water mass shoreward especially in the mid-Atlantic region, including NYC,[73,74] as well as increased frequency of coastal flooding in the Southeast United States.[38]

Projections for SLR in NYC are 14–19 inches (0.36–0.48 m) by the 2050s and 25–39 inches (0.64–0.99 m) by the 2080s when compared with a 1995–2014 baseline period; SLR could reach as high as 5 feet (1.5 m) by 2100. Full details of the methods used to develop these projections with the scenarios shown in Figure 7 can be found in Braneon et al.[24] Under the ARIM scenario presented in 2019 by NPCC3, accelerated loss of land-based ice could lead to SLR of up to 81 inches (2 m) by the 2080s and 114 inches (2.9 m) by 2100 under a plausible "worst-case" scenario that cannot entirely be ruled out.

4 | DRIVERS OF EXTREME HEAT

4.1 | Large-scale drivers

Extreme heat in NYC is driven both by large-scale climate processes and the local characteristics of its land cover. At a large scale, studies show that changes in global mean temperatures have led to an increase in the frequency, intensity, and duration of extreme heat events.[75,76] A review of global drivers of extreme heat by Horton et al.[77] found that several dynamical climate mechanisms impact the occurrence and intensity of extreme heat events such as (1) land-atmosphere feedbacks, (2) atmospheric blocking events, and (3) planetary-scale atmospheric waves. While there is evidence to support that warmer climates may enhance land-atmosphere feedbacks and their impact on heat extremes, there are still open questions on the other aforementioned mechanisms' sensitivity to global climate change.

There is evidence, however, of increasing trends in large-scale circulations linked to extreme heat as a result of global climate change. Horton et al.[78] found increasing trends over North America in the occurrence of warm season atmospheric blocking, often dubbed heat domes for their warm air trapping effect, finding that increases in temperature extremes are impacted not only by thermodynamic changes but also by increased incidence of regional flow regimes. Climate models, however, may have biases in their representation of the incidence of these large-scale flows, which may lead to uncertainties in future projections of extreme heat.[79] Meanwhile, evidence from extreme heat events in Europe indicates that the cooling capacity of soil moisture through evaporation may be

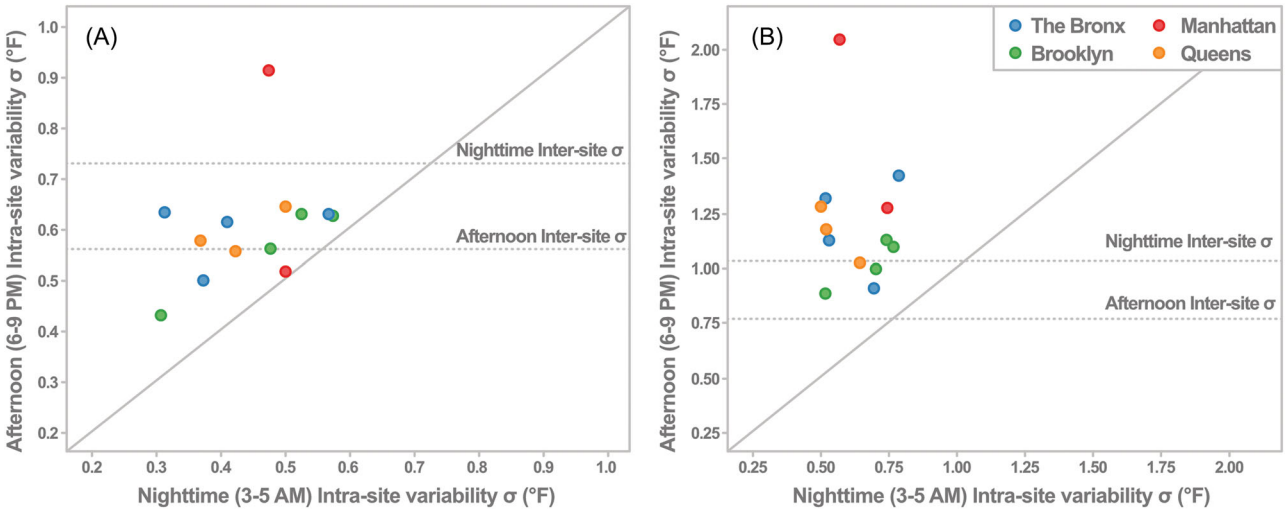

FIGURE 8 Estimates of intrasite under tree canopy air temperature variability (standard deviation [σ]) per borough for (A) summer period (July–August) and (B) upper threshold temperature (>82°F nighttime, 90°F afternoon). Dotted line denotes the intersite variability. Solid line is the 1:1 line. *Source*: NYC DOHMH.

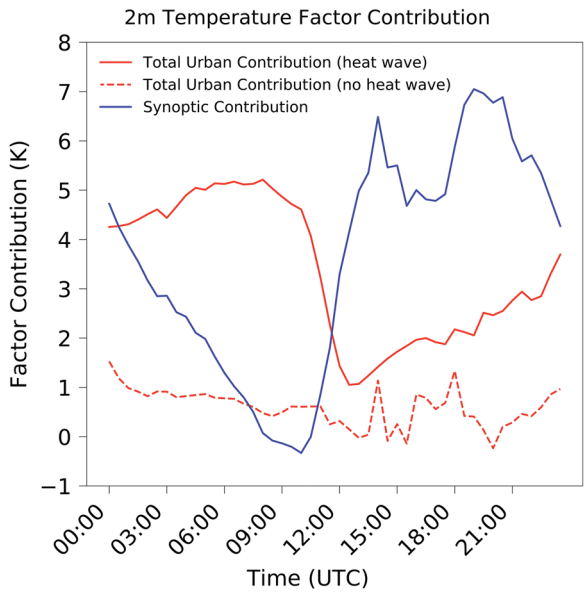

FIGURE 9 Contribution of urban surfaces to near surface temperatures before and during a heat wave event in NYC. Reproduced from Ortiz et al.[101]

depleted by high temperatures, which in turn allows for even higher temperatures due to lack of cooling—a positive feedback.[80] Nevertheless, increased temperatures, including in NYC, are one of the strongest signals in climate projections as a function of increasing GHG emissions.[81]

4.2 | Local drivers

Local landcover characteristics drive surface and air temperature in the urban built and natural environment. The urban built infrastructure refers to streets, sidewalks, and buildings and is primarily comprised of impervious surfaces of varying material types, reflectance, and thermal capacities. Throughout the day, these surfaces retain, store, and emit heat from incoming solar radiation. The rate and magnitude at which the built infrastructure transfers heat impacts the surrounding air and surface temperature of the environment. For example, surfaces that have a low albedo or reflectivity (e.g., asphalt streets) typically absorb and store more heat during the day releasing it slowly as sensible heat in the afternoon.[82] The release of sensible heat warms the surrounding environment. The installation of impervious surfaces in an urban environment such as NYC can also limit natural cooling processes such as evaporation, evapotranspiration, and wind speed and direction.[83] Tall buildings can create an urban canyon effect that can prevent ventilation and trap heat.[82] Anthropogenic heat from human activity like traffic, industrial processes, and air conditioning is an additional source of heat commonly found in the urban environment which can elevate urban air temperature.[82] The natural environment is mainly comprised of pervious surfaces characterized by vegetation like shrubs, grasses, and trees. Vegetation cools the environment through shade and evapotranspiration. The natural environment stores less heat during the day and releases heat at a faster rate than the built environment.

The urban and natural environment store and retain heat from incoming solar radiation throughout the day and commence releasing heat as the sets in the afternoon. The slower release of heat from the built environment creates a temperature differential with areas containing more of the natural environment creating a phenomenon called the Urban Heat Island (UHI)[84] effect characterized by an urban heat island intensity (UHII).[85] UHII is traditionally reported as a temperature difference between the urban and surrounding rural environment. The highest UHII is commonly observed during the late afternoon through the nighttime period. In recent years, other characterizations of UHII have been used in literature[86,87] as a comparison

to include parks,[88,89] airports,[90,91] and land classification zones.[92] In NYC, neighborhoods contain varying amounts of the built and natural infrastructure causing some neighborhoods to maintain warmer temperatures.[93] Equitable heat mitigation and adaptation policies seek to reduce neighborhood temperature heterogeneity while reducing local citywide temperature.[94–96]

UHII in NYC has been studied for several decades, with observations of urban-rural temperature differences of 3.22°F on average and as high as 5.4°F reported by Bornstein.[97] More recent observations based on longer study periods found that the NYC UHII averages between 4°C in the summer and 5.4°C in the winter and spring, with significant variability due to the time of day and prevalent weather conditions.[98]

The spatial distribution of the NYC UHI is linked to both characteristics of the land surface and larger-scale prevailing wind conditions.[99] NYC UHI is impacted significantly by afternoon sea breezes, which move its core inland toward The Bronx and New Jersey in the afternoon, while nighttime land breezes may move its core over Brooklyn and Queens. Studies have found that contributions from NYC's built surface varied significantly due to the characteristics of the urban surface as well as the distance to the southeastern coastline where seabreezes typically come from, and that these contributions extended several hundred meters above the ground.[100,101]

Studies have quantified the impacts of landcover on air temperature in the urban environment. Characteristics of the built environment are more closely associated with nighttime air temperature variance compared to daytime air temperature.[102–105] Minimum (nighttime) air temperature is influenced by building height.[106,107] Research using land use regression modeling has observed a nonlinear relationship between temperature and canopy cover and greenness, requiring a threshold of canopy cover associated with decreases in air temperature, and with diminished cooling as distance increases from tree canopied areas.[105,108] Decreases in nighttime temperatures were found to be associated with a 32% threshold in a 200 m buffer[108] and a greater than 40% threshold in a 60–90 m buffer.[105]

The relationship between urban land cover (i.e., tree canopy, building height/area, impervious land cover) and temperature is made more complex by intra and intervariability based on the time of day.[99] Pedestrian (ground) level air temperature monitoring (see Box 1) offers a means to observe hyperlocal variability to assess and explore microscale interactions between land cover and temperature (see Box 2), which can lead to changes in how humans interact with the environment thus impacting day-to-day human health.

5 | TAIL RISK IMPLICATIONS AND CHALLENGES

Low-probability extreme weather and climate change scenarios that have high consequences are referred to as "tail risk." When assessing the risks associated with natural hazards and climate change, tail risks (i.e., low-probability extreme events) often play a much larger role than the probability of climate hazards alone might indicate.[113] Tail risk is important to quantify, as it entails low-probability scenarios that have high consequences.

Tail risk for extreme weather is often underestimated because the historical record is insufficient to include a good characterization of extreme events. Tail risk for climate projections is often not revealed, due to a focus on the scenarios with moderate GHG emissions (e.g., SSP2-4.5) or by considering 90th percentiles as worst-case scenarios. Uncertainties in tail risk need to be reduced through deeper exploration of historical data, modeling of synthetic events, and climate downscaling simulations. When assessing extreme flooding, tail risk can also be reduced by a more careful extreme value assessment that explores the separation of tropical cyclone (TC) event data from other events.

Underestimating tail risk can lead to repeatedly being caught by surprise by events like Post-tropical Cyclone Sandy (Sandy), the cloudburst associated with the remnants of Hurricane Ida, and potentially other hazards such as extreme winds. Climate change impacts can have high tail risk, such as the ARIM scenario. Baseline (present-day) hazards can also have high tail risk, such as events like Sandy, which can be considered more of a baseline hazard, given that a similar storm surge had occurred in the historical record in 1821,[114] and research has only found anthropogenic climate change to have contributed to 13% (7.5–23%) of the damages.[41] However, Federal Emergency Management Agency (FEMA) and National Oceanic and Atmospheric Administration (NOAA) assessments of extreme coastal water levels at the time of Sandy's impact suggested it was a very unlikely event with a 1570-year recurrence interval.[115,116] Reasons why the tail risk of extreme events such as Sandy and the Ida-remnants cloudburst could be underestimated are revealed below.

5.1 | Extreme precipitation implications

The most direct mechanism of precipitation intensification results from the thermodynamic relationship between atmospheric temperature and the saturation vapor pressure of water, which is known as the Clausius–Clapeyron (CC) relation (warmer air holds more moisture). Under the temperature conditions relevant to weather, the amount of water vapor in the atmosphere at saturation will increase 6–7% per degree Celsius warming. From this thermodynamic relationship alone, it would be expected that precipitation would occur less frequently when the supply of atmospheric moisture is limited, since more moisture would be required for the atmosphere to reach saturation, condense, and precipitate. However, when large-scale weather conditions provide a source of atmospheric moisture, there would be more precipitable water and, in turn, higher rainfall rates once saturation is reached.[117]

Along with this direct thermodynamic effect, climate change can also influence short-duration precipitation extremes through several key atmospheric processes that take place at micro- to global spatial scales. At a global scale, a fundamental effect of global warming will be the thermal expansion of the warming troposphere and stratospheric cooling, resulting in an increase in the height of the tropopause. Increased tropospheric heights will allow for deeper

BOX 1 Temperature monitoring in NYC

In 2018, as a part of Cool Neighborhoods NYC, a comprehensive heat adaptation and mitigation plan,[109] the city launched a 2-year hyper-local temperature monitoring effort installing nearly 500 air temperature sensors in medium to high HVI neighborhoods (see Braneon et al.,[24] Figure 11, for HVI distribution map [2024]). These HVI neighborhoods were identified based on the prevalence of vegetative cover, air conditioning and demographic prevalence, daytime surface temperature, median income, and demographic prevalence. Intra (within) site variability in NYC med-high neighborhoods was observed to be larger during the afternoon when UHII is highest compared to the nighttime (Figure 8A). In contrast, inter (between)-site (between sites) variability is higher at night compared to the afternoon. The magnitude of temperature variability is larger for observations representing higher temperature ranges for the afternoon and nighttime periods (Figure 8B). The site with the highest afternoon variability is Central Harlem, Manhattan adjacent to Marcus Garvey Park. The lowest variability was observed in Stuyvesant Heights Brooklyn. Reducing intra and interneighborhood variability is important when considering equitable heat adaptation and mitigation policies within NYC communities. The thresholds used were based on the 2023 NYC Heat mortality report prepared by the NYC Department of Health and Mental Hygiene.[110]

BOX 2 Interactions between heat waves and UHIs

UHIs are the product of dynamical interactions between the land surface and the atmosphere, as well as urban planning decisions that dictate the form and material properties of urban landscapes. There is significant evidence of UHI intensification during periods of extreme heat due to so-called synergistic interactions.[111] These synergies arise due to (1) the impact of extreme heat on soil moisture availability, which significantly affects the ability of the surface to cool via evapotranspiration, as well as (2) increased intake of heat in built-up surfaces. Studies have found these synergies to also occur in NYC (Figure 9) from Ortiz et al.,[101] with UHI intensification of over 5°C during a heat wave due to limited cooling and enhanced heat storage.[101,112]

convection and increased precipitation rates when local conditions are favorable.[118–120]

Global warming can also influence precipitation patterns through changes in the continental-scale atmospheric circulation patterns that determine the transport of moisture across the globe. In the eastern United States, the climatology of large-scale moisture transport can be described by 16 spatially distinct atmospheric transport patterns, each with a distinct frequency and seasonality.[121] Anthropogenic climate change could potentially alter the frequency or seasonality of these patterns, with implications for local moisture availability and the probability of extreme precipitation in the future.

Large-scale patterns associated with TCs (including tropical depressions, and hurricanes) also play an important role in the climatology of extreme precipitation in the Northeast. This includes events associated with direct rainfall from TCs passing over, or very close to NYC. It also includes extreme rainfall that results from the remnants of tropical storms, such as the cloudburst associated with the remnants of Hurricane Ida in 2021, or changes to atmospheric dynamics such as lifting, instability, or moisture availability induced by TCs hundreds of kilometers away.[122]

In an observational analysis study of the continental United States, Barlow[122] found that over most of the Northeast, more than two-thirds of all extreme daily rainfall events between 1975 and 1999 were linked to TC-related activity. In terms of the dynamics underlying the forcing of extreme precipitation, Barlow's study found that the relationship between TCs or their remnants on large-scale lift was much greater than the relationship with moisture availability and buoyancy. It recommended further study of the interactions of TCs with large-scale circulation patterns that induce lift, such as the jet stream. This is notable, since large-scale lift induced by a powerful jet streak and associated upper-level divergence was a key contributor to the extremely intense precipitation observed during the Ida-remnants cloudburst in NYC in 2021.[123]

The influence of climate change on mesoscale storm processes also has the potential to result in more intense short-duration precipitation. Convective precipitation can occur in isolated thunderstorm cells or as part of organized clusters described as mesoscale (10s–100s of kilometers) convective systems (MCSs), which are often embedded into larger-scale circulation such as squall lines or Nor'easters. Organized convection is associated with increased precipitation efficiency—the ratio of moisture that falls to the surface as precipitation to total condensed moisture within a storm—and more intense precipitation.[67] Mosely et al.[124] found that increased surface temperatures resulted in enhanced convective organization and more extreme precipitation and that, more broadly, the interactions among convective cells could be strongly influenced by large-scale changes in climate.

Historically, flash flooding in the Northeast has been more commonly associated with disorganized, localized convective cells rather than organized MCSs, especially when compared to other regions of the United States.[125] The significance of potential changes in

convective organization in more extreme precipitation with climate change remains uncertain and is still in the early stages of investigation[126]; however, some initial studies indicate that the storm areas may be larger and more organized under climate warming.[118,127] In a climate modeling study simulating an unmitigated global warming scenario (RCP 8.5), Prein et al.[128] found that the total volume of summertime precipitation increased with global warming due to both increased precipitation rates and increases in the area over which precipitation occurs in organized MCSs.

Within individual thunderstorms, the increased moisture from warmer temperatures will increase the release of latent heat, creating more instability and stronger updrafts within thunderstorms and increasing precipitation rates beyond what would be expected from the increase in moisture availability alone. Assuming that latent heat within a thunderstorm is proportional to precipitation intensity and that kinetic energy of rising air within a thunderstorm increases proportionally with latent heating, precipitation intensity would be expected to increase at a rate twice that predicted by the CC relationship alone (2CC-scaling).[118]

Changes in microphysical dynamics within thunderstorm clouds can also influence precipitation efficiency and convective precipitation rates. Precipitation efficiency is determined by the size distribution of hydrometeors (water and ice droplets) within thunderstorm clouds and the extent to which these hydrometeors re-evaporate or are re-entrained in updrafts before falling as precipitation to the ground. Singh and O'Gorman[129] found that climatic warming resulted in an increase in the fall speed of water and ice droplets within clouds. Higher fall speeds reduce the probability that a water droplet will evaporate or be re-entrained in updrafts within the thunderstorm, resulting in higher precipitation efficiency within any given storm. However, the fall speed of water droplets within clouds can also influence updraft velocities, and in-turn precipitation rates.[130,131] Understanding the changes in these microphysical processes are most significant for subhourly precipitation rates;[129] studies on the contribution of TCs to subdaily rainfall in the NYC metropolitan region are not yet available in the academic literature.

5.2 | Sea level rise implications

A key remaining uncertainty around the tail risk of future SLR is the future stability of the ice sheets and the Antarctic Ice Sheet as it holds the equivalent of 58.3 m of GMSLR if all its ice melted. The WAIS is potentially subject to two instabilities: the Marine Ice Sheet Instability (MISI) and Marine Ice Cliff Instability (MICI) (see Braneon et al.,[24] Section 4.1.1). Therefore, in NPCC3, Gornitz et al.[25] also considered one high-end, low-probability scenario—ARIM scenario, which includes these potential instabilities. DeConto et al.,[48] in a revised extreme upper tail GMSLR scenario which also includes these instabilities, found that by 2025, the median contribution of the WAIS to GMSL approaches 1 m and by 2150 rates exceed 6 cm. By 2300, Antarctica could contribute 9.6 m of GMSLR under RCP8.5 due to sustained CO2 emissions increases that extend past 2100.

A new study finds that projected 21st-century ocean temperature increases in the Amundsen Sea region of WAIS point to inevitable widespread basal ice shelf thinning and melting in most GHG emissions scenarios.[132] With weakened ice shelf buttressing, accelerated rates of ice-shelf melting would become inevitable even for moderate future climate policies, with adverse implications for the stability of WAIS.

The Greenland Ice Sheet, which holds the equivalent of 7 meters of SLR, is also potentially vulnerable to abrupt ice-sheet loss beyond a global mean temperature threshold of 1.7 °C–2.3 °C above preindustrial levels.[133] This ice loss can be substantially reduced if global mean temperature change reverts to less than 1.5°C above preindustrial levels within a few centuries. Nevertheless, even temporarily overshooting the 1.5°C temperature threshold, still leads to a peak in SLR of up to several meters even if ice sheets return to nearly historical normals.

5.3 | Potential mischaracterization of tail risk from tropical cyclones

A fundamental challenge with storm-related hazard assessments for the U.S. Mid-Atlantic and southern New England is that tropical cyclones (TCs) (defined as including hybrid storms and post-TCs) are responsible for the largest events (e.g., Sandy and the Ida-remnants cloudburst) but occur infrequently during the typical detailed observation record (e.g., 75 years for hourly rainfall data from 1948 to 2022). Therefore, TC hazard data are typically undersampled, leading to difficulty in constructing extreme value distributions. As a result, despite large differences in TC and extratropical cyclone (ETC), maximum storm intensities judged by pressure drop or maximum sustained wind speed, observation-based assessments of surge, wind and rain hazards typically merge data from TCs with far more numerous data from ETCs. An alternative solution to this problem has been model-based assessments that create synthetic TC events to enable separate extreme value analyses of TCs and ETCs.[114,134] For the NYC area, these model-based assessments that separate data by storm type have at times found substantially higher estimates of water level extremes.[114,135,136] However, such model-based hazard-assessments have a high epistemic uncertainty and are challenging to independently validate. This approach has rarely (or never) been applied for wind and rain hazard assessments for NYC, which have continued to use merged observational data, potentially underestimating the baseline natural hazards and societal tail risk.

A recent analysis is summarized here that evaluates the differences between merged and separate extreme value analyses for TC and ETC storm tides (McPhearson et al.[137], Section 2.9). Storm tide return level data are created for a range of U.S. Mid-Atlantic and Northeast Coast TC and ETC coastal storm tide climates (e.g., Lin et al.[138]; Orton et al.[114]; Dullart et al.[139]). The TC peak storm tide exceedance curves follow the Gumbel distribution with a range of nine different slopes. A single ETC peak storm tide exceedance probability curve is utilized based on the generalized extreme value (GEV) distribution that

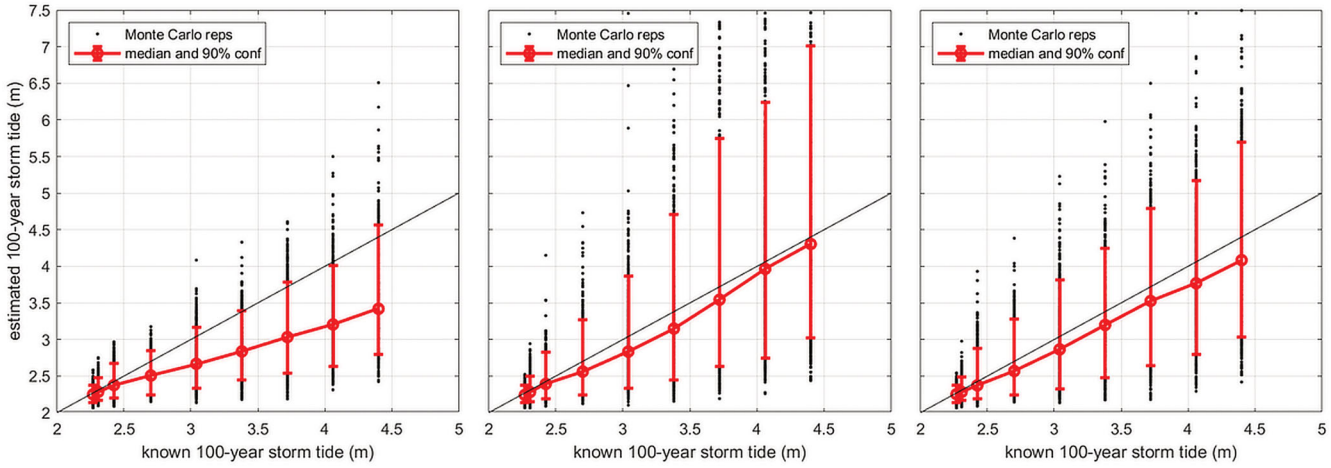

FIGURE 10 Results of a series of Monte Carlo simulations of extreme value analyses of estimated 100-year storm tides for synthetic data for 100-year datasets, across a range of environments with different a priori known 100-year storm tides. EVA approaches studied include (left) GEV distribution fitting of mixed data, (middle) GPD distribution of mixed data, and (right) separated TC and ETC distribution fitting. Error bars show 90% variability ranges of the results.

represents water level extremes for NY Bight and southern New England (e.g., Orton et al.[114]; Dullart et al.[139]).

Stochastic storm tide event sets for TCs and ETCs are created by sampling from these distributions to create synthetic historical periods of 100 years, similar to that available from NOAA for NYC at the Battery tide gauge. One thousand Monte Carlo simulations are performed for each storm tide climate and extreme value analysis (EVA) is applied to each synthetic historical period. In each simulation, EVA is performed on both merged versus separated TC and ETC populations, and the results are compared. Three analysis methods are utilized: (1) fitting combined TC/ETC datasets annual maximum storm tide (AMST) with GEV distributions as has recently been standard practice[116,140]; (2) using a peaks-over-threshold approach and generalized Pareto distribution (GPD) with mixed ETC and TC events, as done in many hazard assessment types (e.g., Atlas-14; others); and (3) using approach #1 for ETC and #2 for fitting TC storm tide distributions.

Results show that fitting GEV distribution to AMST from mixed storm tide populations often leads to underestimated 100-year storm tides (Figure 10, left panel). The GPD approach greatly reduces the low bias (Figure 10, middle panel), but the GPD focus only on the tail of the distribution tail raises the uncertainty higher than that for separated EVA. The separate analysis of TCs and ETCs has moderate uncertainty but minimizes the low bias (Figure 10, right panel).

The results of these analyses demonstrate some of the challenges of quantifying tail risk. Small numbers of extreme events that predominantly come from TCs lead to either low bias or high uncertainty in estimated 100-year extremes, illustrated in Figure 10. These same challenges likely apply to storm surge, wind, and rainfall, and separated EVA should be explored for all these coastal storm-related hazards. These challenges point to the importance of not over-relying on quantitative projections, given deep uncertainties and limitations to model-based projections; more qualitative approaches, grounded in decision-making under uncertainty, are likely to be instructive for these and other uncertainties described in this chapter and throughout this report.

5.4 | Limitations associated with global climate model resolution and downscaling methods

Many recent studies[141–144] have employed a quantile delta approach to develop climate-change-informed IDF curves. Quantiles are discrete segments within a probability distribution, in this context corresponding with the recurrence intervals associated with IDF curves of a given duration.[143] The ensemble of downscaled GCM outputs are used to calculate delta change factors, the relative change between the present, and the future precipitation frequency estimates for each quantile. The delta change factors between historic and future values are calculated separately for each quantile within the IDF probability distribution. This approach is quasi-stationary, with constant delta change factors applied for each future time interval. Time intervals are typically 30 years or more, allowing for representation of multidecadal climate conditions. The delta change factors are then used to adjust IDF curves based on past observations so that they represent future nonstationary climate.

A key advantage of applying the quantile delta change method to calculate the rate of increase of future estimates is that the inherited bias of the climate model data is reduced when applied as ratios. These rates of increase of the future estimates can be applied along with the current period, which is based on more reliable spatial and temporal characteristics of the historical observations.[144] Also, with this approach, the relative changes in all modeled quantiles are accounted for rather than only relative changes in the modeled mean.[145] Future IDF curves were generated using downscaled precipitation data from the Localized Constructed Analogs version 1 (LOCA1)[146] and version

2 (LOCA2)[147] and compared. An ensemble of 21 CMIP5 GCM models is the basis of the LOCA1 dataset, while 27 CMIP6 GCM models, with up to 10 of their ensemble members, are used in LOCA2. Only a single downscaling method was considered given LOCA2 was the only available downscaled CMIP6 dataset available at the time, and due to the desire to reflect data used in the U.S. National Climate Assessment. The two main differences between LOCA1 and LOCA2 are the input GCM data and the precipitation training data——LOCA1 downscaled CMIP5 model outputs, whereas LOCA2 downscaled the CMIP6 models' outputs to generate high-resolution (6 km) future projections of precipitation. LOCA1 used an observational dataset from Cannon et al.;[145] however, additional analyses on this dataset discovered a bias in the strength of daily rain extremes which resulted in unrealistically weak values.[147] LOCA2 uses Pierce et al.,[149] which is believed to correct the bias seen in Livneh et al.[148] and better represent daily rain extremes.[147] Differences in downscaling methodology including the observational data used in bias correction are a source of uncertainty in the resulting projections. Maimone et al.[150] examined the influence of such uncertainty and concluded that despite differences associated with various approaches (including the method used here), the range of future extreme rainfall projections was comparable and provided practical planning-level data.

Overall, a total of six GCM experiments were analyzed. For CMIP5, the historical period covers 1950–2005. Its future climates are based on the representative concentration pathways (RCP) scenarios that represent medium-low emissions (RCP4.5) and high emissions (RCP8.5) future climates. For CMIP6, the historical period covers 1950–2014, and its two future scenarios (2015–2099) under the shared SSPs that represent low emission (SSP245) and high emission (SSP585) future climates.

Across the four stations (Central Park, JFK Airport, LaGuardia Airport, and Newark Airport), the extremes seen in LOCA2 downscaled CMIP6 projections tend to be larger than those in LOCA1 downscaled CMIP5 values in both the lower and high emissions scenarios (Figure 11 B and D). This is particularly evident at the longer recurrence intervals. For Central Park (which is representative of JFK and LaGuardia), the CMIP6 change factors are similar to those from CMIP5 for the 2-year recurrence interval, but for recurrence intervals >5 years, the CMIP6 values exceed the 50% confidence interval of the CMIP5 (LOCA1) values in the majority of cases (Figure 11A and B). The results for Newark are similar (Figure 11C and D). Like Central Park, the CMIP6 2-year recurrence interval change factor is marginally lower than that of CMIP5, but for the remaining returning periods, the CMIP6 values exceed those from CMIP5. However, Newark is the only station where all CMIP6 change factors are within the 50% confidence interval of CMIP5 (Figure 11C and D). It should be noted that these differences can arise from both the underlying GCMs as well as the differences in methods used in LOCA1 and LOCA2.

The GCMs downscaled to develop the delta change factors are able to represent the dynamics of large-scale atmospheric processes and their interactions across the globe. But they are unable to represent the dynamic processes described in Section 5.2.1 that take place at finer-spatial scales (Table 4).[63,151] While statistical downscaling provides a means to represent the finer-scale spatial structure of precipitation, it is based on historical patterns that may not be representative of future climate. For example, the observed changes in annual probability for extreme subdaily precipitation at the Central Park Weather Station are substantially greater than those for daily precipitation (Table 3). Such changes may not be represented in current projections based on downscaled GCMs if they result from finer-scale processes.

As an alternative, convection permitting regional climate models (CPRCMs) are RCMs run at < 4 km spatial resolution. At this resolution, deep convection parameterization is no longer required since the convective dynamics within rainstorms—and their potential changes with global warming—can be explicitly simulated.[148–152] In addition, these models are better able to represent details of the land surface, which might be particularly important in highly urbanized areas like NYC.[153,154] But while CPRCMs have the potential to provide important insight on how climate change will impact extreme precipitation, no single CPRCM can accurately represent future climate on its own and studies utilizing an ensemble of CPRCM outputs are needed to generate robust projections for subdaily precipitation.[155,156] The computational expense of CPCRM remains a challenge and such studies have only been piloted in a small number of regions across the world over the last 4 years.[157] At the time of writing, an ensemble of CPCRM forecasts needed to conduct such a study is not yet available for NYC.

6 | OPPORTUNITIES FOR FUTURE RESEARCH

There remain key gaps in the understanding of changing climate risks in NYC. In this section, we present a nonexhaustive list of research gaps that may inform important impacts of a changing climate in NYC, tied to the topics covered here. Additional research gaps related to climate and its changing impacts may be found in Braneon et al.[24] While projections for extreme heat were updated in this chapter, they focused on outdoor conditions as modeled by climate models in CMIP6. However, indoor heat exposure remains the most common site for the onset of heat-related mortality and hospitalizations.[158] Addressing this gap will need an interdisciplinary research agenda that studies not only the physics of the climate systems but also its interactions with human infrastructure (e.g., homes, the urban canopy). Another gap related to extreme heat is the lack of spatially explicit projections for air temperature. NPCC3[26] described new methods that could fill this gap using methods like dynamical downscaling, but high computational costs and uncertainties around future changes to the city's urban landscape have made robust application prohibitive. Downscaled projections to the neighborhood and higher levels could provide invaluable information on the physical interactions between a changing climate and the unjust distribution of heat-resilient spaces that lead to inequitable exposure to extreme heat in cities like NYC.[6,158–160]

Another key gap relates to the treatment of CMIP6 models with ECS outside of the likely range. Although the analysis presented in this chapter describes the existing differences between the so-called hot models and the rest of the CMIP6 ensemble, there may be larger-scale physical processes that may be poorly constrained in

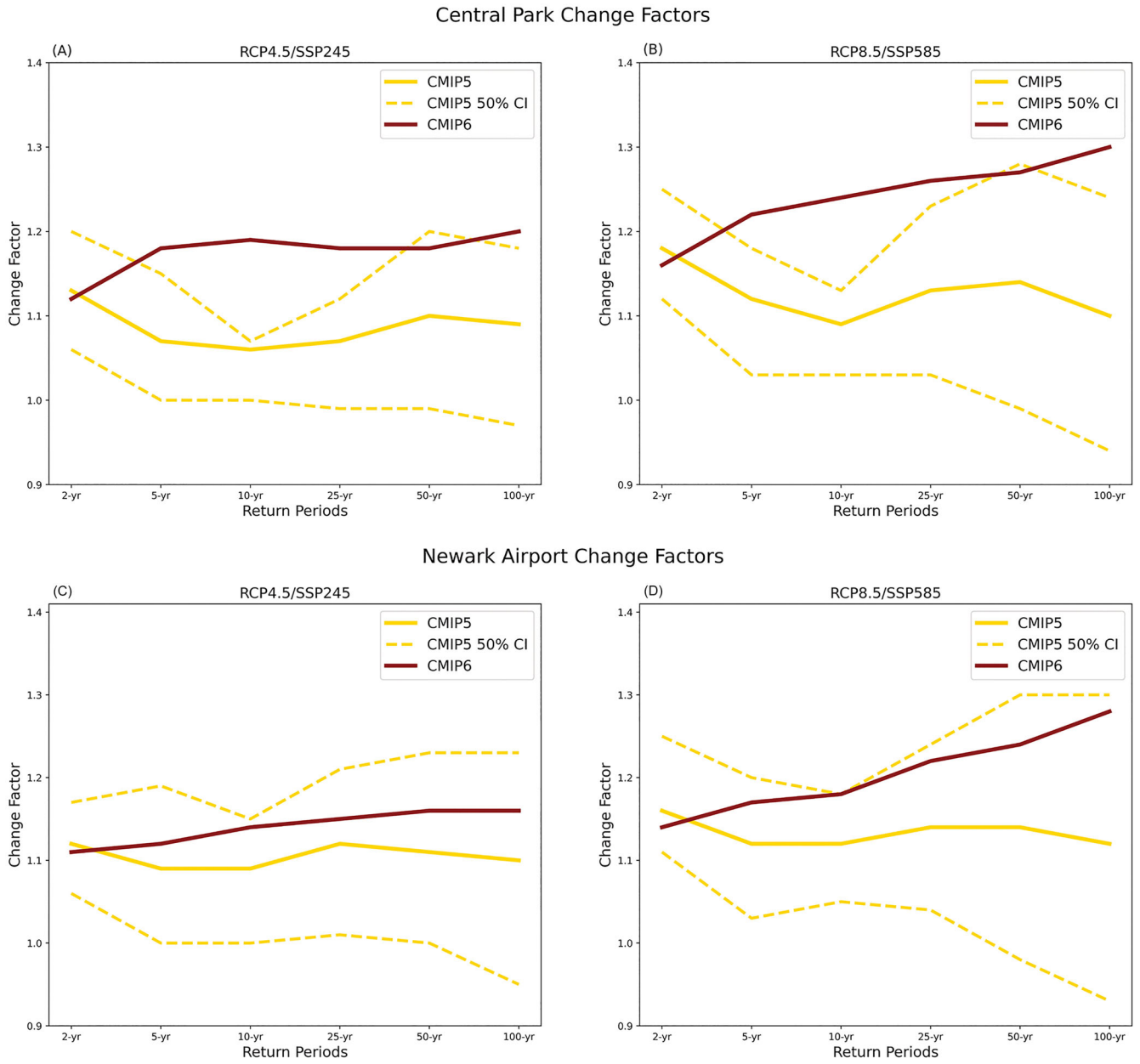

FIGURE 11 Comparison of CMIP5 and CMIP6 extremes for multiple recurrence intervals (return periods) and across medium-low (RCP4.5) and high (RCP8.5) emissions scenarios. Solid lines denote ensemble means, while dashed lines show the ensemble 50% confidence interval. *Source*: NCEI Hourly Precipitation Dataset and Local Climatological Dataset.

these models. Additional research may be needed to better understand the relationships between increased ECS and the frequency and intensity of weather extremes in NYC. Moreover, because of the complex nature of the climate system and the models that try to quantify their processes, the causes of enhanced ECS are poorly understood. A research agenda that includes out-of-sample tests from paleoclimate records and modeling may provide insights into the constraints needed in the next generations of earth systems models.[161] Similarly, data collection on key processes related to large-scale drivers of climate change and sea level rise may inform constraints on existing models and improve estimation across a range of impacts. As an intermediate solution, future NPCC assessments could elect to present projections across global warming levels (e.g., 2°C, 3°C) to avoid some of the potential influences from the "hot models" in the CMIP ensemble.

7 | TRACEABLE ACCOUNTS

Key Message 1 NPCC4 analysis of the impact of hot models on the CMIP6 ensemble found no statistically significant difference between the temperature and precipitation projections of record and alternative projections that do not include models with ECS outside the expected range. The CMIP6 climate model ensemble used to

TABLE 4 Representation of multiscale precipitation processes in climate models.

Climate model type [spatial resolution]	General circulation model (GCMs) [25—100 km]	Tropical cyclone permitting GCMs [20—50 km]	Regional climate model (RCMs: e.g., NA-CORDEX) [25—50 km]	Convection permitting RCMs [1—4 km]
Thermodynamic processes	CC-scaling with global covariates (radiative forcing, mean global temperature anomaly)	CC-scaling with global covariates (radiative forcing, mean global temperature anomaly)	CC-scaling with local covariates (local temperature, dewpoint, precipitable water)	CC-scaling with local covariates (local temperature, dewpoint, precipitable water)
Increased tropopause height	Represented in convection parameterizations	Represented in convection parameterizations	Represented in convection parameterizations	Represented in model simulations
Large (continental)-scale atmospheric circulation patterns and moisture transport	Represented in model simulations	Represented in model simulations	Provided as lateral boundary conditions from GCMs	Provided as lateral boundary conditions from GCMs
Tropical cyclones	Insufficiently represented	Represented in model simulations	Represented in model simulations	Represented in model simulations
Mesoscale changes to convective organization	Not directly represented	Not directly represented	Not directly represented	Represented in model simulations
Within-storm convective processes	Not directly represented	Not directly represented	Not directly represented	Represented in model simulations

create the temperature and precipitation projections of record contains three models that display higher-than-expected sensitivity of temperatures to GHGs. These so-called hot models lead to higher global mean temperatures. However, the impact of high climate sensitivity appears small with our approach to developing local projections for NYC. Nevertheless, more research is needed to better understand (1) the impact of the high climate sensitivity on the representation of key large-scale climate processes, (2) the model physics leading to high sensitivity in the first place, and (3) the constraints on the planet's ECS.

- **Description of Evidence**: Many models that make up the CMIP6 experiment and serve as the basis of NPCC projections of record are more sensitive to GHG forcing than previous generations of models, leading to hotter global average temperatures.[30] This higher sensitivity is often attributed to stronger positive cloud feedbacks from decreasing extratropical low cloud coverage and albedo.[30] Analysis by NPCC4 found nonstatistically significant differences between projections of record when hot models are removed.
- **New Information and Remaining Uncertainties**: Although high sensitivity models are still within the likely ECS range as supported by evidence,[162] there is evidence from the paleorecord indicating that such high values are unrealistic.[163] New evidence from paleoclimate records and simulations may be needed to better constrain the newer generation of earth system models.[164]
- **Assessment of Confidence based on the Evidence**: Given the analysis performed by NPCC4, there is high confidence that the projections of record presented in Braneon et al.[24] are not significantly impacted by the hot model problem. There is medium confidence that the representations of all physical processes relevant to the climate of NYC are not significantly impacted by these high ECS models.

Key Message 2 The high tail end of SLR will be governed by the future stability of the WAIS and Greenland ice sheets throughout the 21st century and beyond. If all marine-based ice melted, the WAIS could contribute ~3m, and the Greenland Ice Sheet ~7 m of SLR potential. Troubling signs of ice shelf thinning and ocean warming around the WAIS and an approaching temperature tipping point over Greenland raise the possibility of faster and higher SLR than projected by most climate models, increasing the risks associated with coastal flooding. Additional research is needed to gain a better understanding of all the processes governing ice sheet behavior with rising temperatures. Stakeholders concerned with long-term planning need to examine plausible scenarios at the extreme upper tail of the SLR distribution.

- **Description of Evidence**: MISI may develop because much of the WAIS lies on land below sea level, on reverse slopes that tilt toward the continental interior—an inherently unstable topographic configuration. An ice stream or glacier on a reverse slope near the grounding line undergoing MISI accelerates, calving more and more ice until the bed slope flattens or rises landward (e.g., Figure 3.5 in Gornitz et al.)[25,164] A more controversial process is the MICI in which the exposed cliff face of a high ice cliff (>100 m [~328 ft] above sea level) may become structurally weakened and collapse after thinning and removal of a buttressing ice shelf. Furthermore, in a warmer climate, larger meltwater pools on top of an ice cliff during summer would propagate down crevasses and cut through ice until reaching bottom in a process known as hydrofracturing. Ice cliff retreat is accelerated as large ice masses calve. Several regions of the WAIS face high vulnerability to (marine ice shelf instability) MISI. In particular, the Thwaites Glacier would become "unstoppable" once it passes beyond two ridges.[165] If current rates of retreat persist, the Thwaites Eastern Ice Shelf (TEIS) could unpin from the seafloor in less than a decade. The collapse of Thwaites Glacier, which holds

the equivalent of more than half a meter of global SLR potential, could also destabilize neighboring glaciers that hold another 3 m of SLR potential. Three other glaciers near Thwaites show rapid retreat within the last decade.[164]

- **New Information and Remaining Uncertainties**: A recent study confirms the ongoing rapid retreat of the Thwaites Glacier's grounding line, in particular near a pinning point mapped in 2014.[163–166] New underwater surveys of the TEIS between 2011 and 2020 also reveal favorable submarine topography that promotes enhanced melting near the ice base and entry of warmer ocean water leading to sustained grounding line retreat.[167] On the other hand, negative feedbacks, such as glacial rebound or a weakened gravitational attraction, may mitigate the full extent of MISI.[168,169] MICI may be delayed by slower retreat of ice shelves,[170] rates and degree of effectiveness of hydrofracturing,[171] and lack of evidence for an observed MICI either at present or in the geological past.[172]
- **Assessment of Confidence based on the Evidence**: Recent ice sheet observations raise renewed concerns over the long-term stability of both the WAIS and Greenland Ice Sheet with continued climate warming. Glaciers and ice sheets combined are now the dominant contributors to GMSLR with very high confidence. Further, sea level is projected to rise for centuries and remain elevated for thousands of years with very high confidence.

Key Message 3 While the occurrence of extreme heat events in NYC is governed in great part by climatic events taking place at large spatial scales, local urbanization patterns play a key role in the spatial distribution of temperatures within the city. These local patterns, which include a range of factors like distribution of green spaces and urban geometry, play the most significant role in the generation of physical process that lead to the UHI. Moreover, extreme heat events exacerbate this intraurban excess temperatures, increasing exposure to deadly heat of populations without access to adaptive measures and cooling infrastructure (e.g., cooling centers, tree shade). Future work is needed to assess the impact of a warming climate on intraurban heat variability in order to quantify the effect of climate change on spatial inequities of heat exposure.

- **Description of Evidence**: The NYC UHI has been studied for decades, with measurements of urban-rural temperature differences going back decades.[97] There is significant evidence of the impact of urban surfaces on temperatures in NYC, with values often ranging between 0.5 and 5 depending on the time of year and prevailing weather conditions.[98,173] Further, there is significant evidence of positive feedbacks between the NYC UHI and extreme heat events.[101,112]
- **New Information and Remaining Uncertainties**: Although most studies have shown intensification of UHIs during extreme heat events, some have found no such intensification in the observation record.[174] Further, there are robust projections of intraurban heat in NYC that account for local physics across model ensembles and climatologically relevant temporal scales.
- **Assessment of Confidence based on the Evidence**: Given the significant modeling and observational evidence, there is very high confidence in the existence and magnitude of the NYC UHI. There is also high confidence of synergistic interactions between extreme heat and UHIs, although the extent of these interactions remains a topic of research.

ACKNOWLEDGMENTS AND CONTRIBUTORS

This assessment does not represent the policy position of any agencies whose staff are co-authors.

The authors are grateful for the constructive remarks of Richard Moss and Jack Tchen. The authors are thankful for the funding for interns, fellows, and workshops that was provided by Columbia University, The New School, Sarah Lawrence College, Rutgers University, and the City University of New York. Timon McPhearson acknowledges funding from the National Science Foundation (Grants #1444755, #1927167, and #193493). Christian Braneon acknowledges funding from the AXA Research Fund.

Kathryn McConnell was supported by the National Science Foundation Human-Environment and Geographical Sciences (HEGS) and Sociology Programs through award number 2117405, titled Analysis of Impacts of Environmental and Natural Hazards on Human Migration (awarded to E. Fussell, Brown University, J. DeWaard, Population Council and University of Minnesota, K. Curtis, University of Wisconsin-Madison, and J. Schroeder, University of Minnesota). She was further supported by the Population Studies and Training Center at Brown University through the generosity of the Eunice Kennedy Shriver National Institute of Child Health and Human Development (P2C HD041020). Any opinions, findings, and conclusions or recommendations expressed in this material are those of the authors and do not necessarily reflect the views of the NSF or NASA.

NPCC Climate Science and Projections Workgroup Co-chairs

- Christian Braneon, PhD (NPCC4 Panel Co-chair; Climate Science & Projections Working Group Co-chair), Research Scientist at CUNY Institute for Demographic Research at the City University of New York; Research Physical Scientist at NASA Goddard Institute for Space Studies, New York, NY; Adjunct Assistant Professor of Climate at Columbia Climate School.
- Luis Ortiz, PhD (NPCC Climate Science & Projections Working Group Co-chair), Assistant Professor, George Mason University, Fairfax, VA.

NPCC Climate Science and Projections Workgroup Panel Members and Scientific Contributors

- Dan Bader, MA, NASA Goddard Institute for Space Studies, New York, NY.
- Maya Buchanan, PhD, WSP USA, Portland, OR.
- LaTonya Carter, MS, Department of Geography and Geospatial Science, George Mason University, Fairfax, VA.
- Colin Evans, PhD, Cornell University

- Art DeGaetano, PhD, Professor, Department of Earth and Atmospheric Sciences, Cornell University
- Vivien Gornitz, PhD, NASA Goddard Institute for Space Studies, New York, NY.
- Sanketa Kadam, MS, MA, Columbia University, New York, NY.
- Radley Horton, PhD (NPCC4 Panel Member) Research Professor, Columbia University Lamont-Doherty Earth Observatory.
- Evan Mallen, PhD, Urban Climate Lab, School of City and Regional Planning, Georgia Institute of Technology, Atlanta, GA.
- Talea Mayo, PhD, Emory University, Atlanta, GA.
- Kathryn McConnell, PhD, The University of British Columbia, Vancouver, British Columbia, CA.
- Timon McPhearson, PhD (NPCC4 Futures & Transitions Working Group Co-chair, Climate Science & Projections and Flooding Working Group Member), Professor, Urban Ecology and Director, Urban Systems Lab, The New School.
- Franco Montalto, PhD (NPCC4 Panel Member and Flooding Working Group Co-chair), Professor, Civil, Architectural and Environmental Engineering, Drexel University, Philadelphia, PA.
- Philip Orton, PhD (NPCC4 Panel Member) Research Associate Professor, Ocean Engineering, Stevens Institute of Technology.
- Mobin Rahimi-Golkhandan, MS, Drexel University, Philadelphia, PA
- Bernice Rosenzweig, PhD (NPCC4 Flooding Working Group Co-chair) Faculty Member, Environmental Science, Sarah Lawrence College.
- Hadia Sheerazi, MSc, Rocky Mountain Institute, New York, NY.

Interagency Climate Advisory Team (ICAT) Members

- Lauren Smalls-Mantey, PhD, NYC Department of Health & Mental Hygiene, New York, NY.

External advisors

- Cuihua Li, Columbia University Lamont-Doherty Earth Observatory.

Other contributors

- Janice Barnes, PhD, Managing Partner, Climate Adaptation Partners, New York, NY.
- Hayley Elszasz, PhD, Climate Science Advisor, Mayor's Office of Climate and Environmental Justice, New York, NY.
- Leo Temko, MSc, General Partner, Climate Adaptation Partners, New York, NY.

COMPETING INTERESTS

The authors declare no competing interests.

ORCID

Luis Ortiz https://orcid.org/0000-0002-4248-6374
Christian Braneon https://orcid.org/0000-0003-1878-1397

REFERENCES

1. Boeckmann, M., & Zeeb, H. (2016). Justice and equity implications of climate change adaptation: A theoretical evaluation framework. *Healthcare*, *4*, 65. https://doi.org/10.3390/healthcare4030065
2. Foster, S., Leichenko, R., Nguyen, K. H., Blake, R., Kunreuther, H., Madajewicz, M., Petkova, E. P., Zimmerman, R., Corbin-Mark, C., Yeampierre, E., Tovar, A., Herrera, C., & Ravenborg, D. (2019). New York City Panel on Climate Change 2019 Report Chapter 6: Community-Based Assessments of Adaptation and Equity. *Annals of the New York Academy of Sciences*, *1439*, 126–173. https://doi.org/10.1111/nyas.14009
3. Easton, M., Carrodus, G., Wilson, J., Wilson, A., Ryan, M., Thomson, K., Smith, R., & Davey, K. (2022). Chapter 7: Introduction to the Industrial Revolution. In *Oxford Humanities*. Oxford University Press.
4. Sachs, J. (2020). *America's Zero Carbon Action Plan*. Sustainable Development Solutions Network (SDSN).
5. Baker, W. O. (2019). *Dissonances of Dispossession: Narrating Colonialism and Slavery in the Expansion of Capitalism* (Doctoral dissertation, The University of New Mexico).
6. Foster, S., Baptista, A., Nguyen, K. H., Tchen, J., Tedesco, M., & Leichenko, R. (2024). NPCC4: Advancing climate justice in climate adaptation strategies for New York City. *Annals of the New York Academy of Sciences*.
7. Munshi, S. (2022). Dispossession: An American property law tradition. *Georgetown Law Journal*, *110*, 1021–1096.
8. Park, K. S. (2022). The history wars and property law: Conquest and slavery as foundational to the field. *Yale Law Journal*, *131*, 1062–1384.
9. Tchen, J. K. W. (2001). *New York before Chinatown: Orientalism and the shaping of American culture, 1776–1882* (Paperbacks ed.). Johns Hopkins University Press.
10. Táíwò, O. O. (2022). *Reconsidering reparations: Worldmaking in the case of climate crisis*. Oxford University Press.
11. Whyte, K. (2017). Indigenous climate change studies: Indigenizing futures, decolonizing the Anthropocene. *English Language Notes*, *55*, 153–162. https://doi.org/10.1215/00138282-55.1-2.153
12. Braveman, P. A., Arkin, E., Proctor, D., Kauh, T., & Holm, N. (2022). Systemic and structural racism: Definitions, examples, health damages, and approaches to dismantling. *Health Affairs*, *41*, 171–178. https://doi.org/10.1377/hlthaff.2021.01394
13. Egede, L. E., Walker, R. J., Campbell, J. A., Linde, S., Hawks, L. C., & Burgess, K. M. (2023). Modern day consequences of historic redlining: Finding a path forward. *Journal of General Internal Medicine*, *38*, 1534–1537. https://doi.org/10.1007/s11606-023-08051-4
14. Farrell, J., Burow, P. B., Mcconnell, K., Bayham, J., Whyte, K., & Koss, G. (2021). Effects of land dispossession and forced migration on Indigenous peoples in North America. *Science*, *374*, eabe4943. https://doi.org/10.1126/science.abe4943
15. Lynch, E. E., Malcoe, L. H., Laurent, S. E., Richardson, J., Mitchell, B. C., & Meier, H. C. S. (2021). The legacy of structural racism: Associations between historic redlining, current mortgage lending, and health. *SSM - Population Health*, *14*, 100793. https://doi.org/10.1016/j.ssmph.2021.100793
16. Pörtner, H. O., Roberts, D. C., Poloczanska, E. S., Mintenbeck, K., Tignor, M., Alegria, A., Craig, M., Langsdorf, S., Loschke, S., Moller, V., Okem, A., & B. Rama (Eds.), *Climate Change 2022 – Impacts, Adaptation and Vulnerability: Working Group II Contribution to the Sixth Assessment Report of the Intergovernmental Panel on Climate Change* (1st ed.). Cambridge University Press. 3–33. https://doi.org/10.1017/9781009325844
17. Sultana, F. (2022). The unbearable heaviness of climate coloniality. *Political Geography*, *99*, 102638. https://doi.org/10.1016/j.polgeo.2022.102638
18. Field, C. B., Barros, V. R., Mach, K. J., Mastrandrea, M. D., Aalst, M. K., van Adger, W. N., Arent, D. J., Barnett, J., Betts, R. A., Bilir, T. E., Birkmann, J., Carmin, J., Chadee, D. D., Challinor, A. J., Chatterjee, M., Cramer, W., Davidson, D. J., Estrada, Y. O., Gattuso, J. -P., … L. L. White (Eds.), *Climate Change 2014: Impacts, Adaptation, and Vulnerability. Part A: Global and Sectoral Aspects. Contribution of Working*

Group II to the Fifth Assessment Report of the Intergovernmental Panel on Climate Change (pp. 35–94). Cambridge University Press.
19. Hoffman, J. S., Shandas, V., & Pendleton, N. (2020). The effects of historical housing policies on resident exposure to intra-urban heat: A study of 108 US urban areas. *Climate*, *8*, 1–15.
20. Buchanan, M. K., Kulp, S., Cushing, L., Morello-Frosch, R., Nedwick, T., & Strauss, B. (2020). Sea level rise and coastal flooding threaten affordable housing. *Environmental Research Letters*, *15*, 1–15.
21. City of New York. (2012). *Local Law 42*.
22. Rosenzweig, C., & Solecki, W. (2015). Preface to Building the Knowledge Base for Climate Resiliency: New York City Panel on Climate Change 2015 Report. *Annals of the New York Academy of Sciences*, *1336*, 7. https://doi.org/10.1111/nyas.12653
23. Rosenzweig, C., Solecki, W., College, H., Blake, R., Bowman, M., Gornitz, V., Jacob, K., Kinney, P., Kunreuther, H., Kushnir, Y., Leichenko, R., Lin, N., Nordenson, G., Oppenheimer, M., Yohe, G., Horton, R., Lead, C., Patrick, L., Bader, D., … Ali, S. (2013). *New York City Panel on Climate Change—Climate Risk Information 2013: Observations, Climate Change Projections, and Maps*. City of New York. https://climate.cityofnewyork.us/reports/climate-risk-information-2013-observations-climate-change-projections-and-maps-new-york-city-panel-on-climate-change/
24. Braneon, C., Ortiz, L., Bader, D., Devineni, N., Orton, P., Rosenzweig, B., Mcphearson, T., Smalls-Mantey, L., Gornitz, V., Mayo, T., Kadam, S., Sheerazi, H., Glenn, E., Yoon, L., Derras-Chouk, A., Towers, J., Leichenko, R., Balk, D., Marcotullio, P., & Horton, R. (2024). New York City climate risk information 2022—observations and projections. Annals of the New York Academy of Sciences, 1–36.
25. Gornitz, V., Oppenheimer, M., Kopp, R., Orton, P., Buchanan, M., Lin, N., Horton, R., & Bader, D. (2019). New York City Panel on Climate Change 2019 Report Chapter 3: Sea Level Rise. *Annals of the New York Academy of Sciences*, *1439*, 71–94. https://doi.org/10.1111/nyas.14006
26. González, J. E., Ortiz, L., Smith, B. K., Devineni, N., Colle, B., Booth, J. F., Ravindranath, A., Rivera, L., Horton, R., Towey, K., Kushnir, Y., Manley, D., Bader, D., & Rosenzweig, C. (2019). New York City Panel on Climate Change 2019 Report Chapter 2: New Methods for Assessing Extreme Temperatures, Heavy Downpours, and Drought. *Annals of the New York Academy of Sciences*, *1439*, 30–70. https://doi.org/10.1111/nyas.14007
27. New York State Energy Research and Development Authority. (2024). New York State Climate Impacts Assessment. https://nysclimateimpacts.org/
28. Ebi, K. L., Hallegatte, S., Kram, T., Arnell, N. W., Carter, T. R., Edmonds, J., Kriegler, E., Mathur, R., O'neill, B. C., Riahi, K., Winkler, H., Van Vuuren, D. P., & Zwickel, T. (2014). A new scenario framework for climate change research: Background, process, and future directions. *Climatic Change*, *122*, 363–372. https://doi.org/10.1007/s10584-013-0912-3
29. O'neill, B. C., Tebaldi, C., Van Vuuren, D. P., Eyring, V., Friedlingstein, P., Hurtt, G., Knutti, R., Kriegler, E., Lamarque, J. F., Lowe, J., Meehl, G. A., Moss, R., Riahi, K., & Sanderson, B. M. (2016). The Scenario Model Intercomparison Project (ScenarioMIP) for CMIP6. *Geoscientific Model Development*, *9*, 3461–3482. https://doi.org/10.5194/gmd-9-3461-2016
30. Zelinka, M. D., Myers, T. A., Mccoy, D. T., Po-Chedley, S., Caldwell, P. M., Ceppi, P., Klein, S. A., & Taylor, K. E. (2020). Causes of higher climate sensitivity in CMIP6 models. *Geophysical Research Letters*, *47*, e2019GL085782. https://doi.org/10.1029/2019GL085782
31. Panofsky, H. A., & Brier, G. W. (1968). Some applications of statistics to meteorology.
32. Kopp, R. E., Garner, G. G., Hermans, T. H. J., Jha, S., Kumar, P., Slangen, A. B. A., Turilli, M., Edwards, T. L., Gregory, J. M., Koubbe, G., Levermann, A., Merzky, A., Nowicki, S., Palmer, M. D., & Smith, C. (2023). *The Framework for Assessing Changes To Sea-level (FACTS) v1.0-rc: A platform for characterizing parametric and structural uncertainty in future global, relative, and extreme sea-level change*. Climate and Earth System Modeling. https://doi.org/10.5194/egusphere-2023-14
33. National Oceanic and Atmospheric Administration (NOAA). (2023). NOAA Tides & Currents. https://tidesandcurrents.noaa.gov/stationhome.html?id=8518750
34. National Oceanography Centre. (2023). Permanent Service for Mean Sea Level (PSMSL). https://psmsl.org/
35. Intergovernmental Panel on Climate Change (IPCC). (2023). Ocean, Cryosphere and Sea Level Change. In Climate Change 2021 — The Physical Science Basis: Working Group I Contribution to the Sixth Assessment Report of the Intergovernmental Panel on Climate Change (pp. 1211–1362). chapter, Cambridge: Cambridge University Press.
36. Buzzanga, B., Bekaert, D. P. S., Hamlington, B. D., Kopp, R. E., Govorcin, M., & Miller, K. G. (2023). Localized uplift, widespread subsidence, and implications for sea level rise in the New York City metropolitan area. *Science Advances*, *9*, eadi8259. https://doi.org/10.1126/sciadv.adi8259
37. Little, C. M., Hu, A., Hughes, C. W., Mccarthy, G. D., Piecuch, C. G., Ponte, R. M., & Thomas, M. D. (2019). The relationship between U.S. East Coast sea level and the Atlantic Meridional Overturning Circulation: A review. *Journal of Geophysical Research: Oceans*, *124*, 6435–6458. https://doi.org/10.1029/2019JC015152
38. Volkov, D. L., Zhang, K., Johns, W. E., Willis, J. K., Hobbs, W., Goes, M., Zhang, H., & Menemenlis, D. (2023). Atlantic meridional overturning circulation increases flood risk along the United States southeast coast. *Nature Communications*, *14*, 5095. https://doi.org/10.1038/s41467-023-40848-z
39. Wunderling, N., Donges, J. F., Kurths, J., & Winkelmann, R. (2021). Interacting tipping elements increase risk of climate domino effects under global warming. *Earth System Dynamics*, *12*, 601–619. https://doi.org/10.5194/esd-12-601-2021
40. Sweet, W., Hamlington, B. D., Kopp, R. E., Weaver, C. P., Barnard, P. L., Bekaert, D., Brooks, W., Craghan, M., Dusek, G., Frederikse, T., Garner, G., Genz, A. S., Krasting, J. P., Larour, E., Marcy, D., Marra, J. J., Obeysekera, J., Osler, M., Pendleton, M., … Zuzak, C. (2022). *Global and regional sea level rise scenarios for the United States*. National Oceanic and Atmospheric Administration.
41. Strauss, B. H., Orton, P. M., Bittermann, K., Buchanan, M. K., Gilford, D. M., Kopp, R. E., Kulp, S., Massey, C., Moel, H. D., & Vinogradov, S. (2021). Economic damages from Hurricane Sandy attributable to sea level rise caused by anthropogenic climate change. *Nature Communications*, *12*, 2720. https://doi.org/10.1038/s41467-021-22838-1
42. National Aeronautics and Space Administration. (2023). NASA Sea Level Change Portal. https://sealevel.nasa.gov/ipcc-ar6-sea-level-projection-tool?psmsl_id=12&data_layer=scenario
43. Gornitz, V., Lebedeff, S., & Hansen, J. (1982). Global sea level trend in the past century. *Science*, *215*, 1611–1614. https://doi.org/10.1126/science.215.4540.1611
44. Mercer, J. H. (1978). West Antarctic ice sheet and CO2 greenhouse effect: A threat of disaster. *Nature*, *271*, 321–325. https://doi.org/10.1038/271321a0
45. Oppenheimer, M., Oreskes, N., Jamieson, D., Brysse, K., O'Reilly, J., Shindell, M., & Wazeck, M. (2019). *Discerning experts: The practices of scientific assessment for environmental policy*. University of Chicago Press.
46. Garner, G. G., Hermans, T., Kopp, R. E., Slangen, A. B. A., Edwards, T. L., Levermann, A., Nowicki, S., Palmer, M. D., Smith, C., Fox-Kemper, B., Hewitt, H. T., Xiao, C., Aðalgeirsdóttir, G., Drijfhout, S. S., Golledge, N. R., Hemer, M., Krinner, G., Mix, A., Notz, D., … Pearson, B. (2021). IPCC AR6 Sea Level Projections. https://doi.org/10.5281/ZENODO.5914709

47. Bamber, J. L., Oppenheimer, M., Kopp, R. E., Aspinall, W. P., & Cooke, R. M. (2019). Ice sheet contributions to future sea-level rise from structured expert judgment. *Proceedings of the National Academy of Sciences of the United States of America*, *116*, 11195–11200. https://doi.org/10.1073/pnas.1817205116
48. Deconto, R. M., Pollard, D., Alley, R. B., Velicogna, I., Gasson, E., Gomez, N., Sadai, S., Condron, A., Gilford, D. M., Ashe, E. L., Kopp, R. E., Li, D., & Dutton, A. (2021). The Paris Climate Agreement and future sea-level rise from Antarctica. *Nature*, *593*, 83–89. https://doi.org/10.1038/s41586-021-03427-0
49. Bassis, J. (2021). Eos. http://eos.org/opinions/quit-worrying-about-uncertainty-in-sea-level-projections
50. Hausfather, Z., Marvel, K., Schmidt, G. A., Nielsen-Gammon, J. W., & Zelinka, M. (2022). Climate simulations: Recognize the 'hot model' problem. *Nature*, *605*, 26–29. https://doi.org/10.1038/d41586-022-01192-2
51. Rypdal, M., Boers, N., Fredriksen, H. B., Eiselt, K. U., Johansen, A., Martinsen, A., Falck Mentzoni, E., Graversen, R. G., & Rypdal, K. (2021). Estimating remaining carbon budgets using temperature responses informed by CMIP6. *Frontiers in Climate*, *3*, 1–14. https://doi.org/10.3389/fclim.2021.686058
52. Massoud, E. C., Lee, H. K., Terando, A., & Wehner, M. (2023). Bayesian weighting of climate models based on climate sensitivity. *Communications Earth & Environment*, *4*, 365. https://doi.org/10.1038/s43247-023-01009-8
53. Weigel, A. P., Knutti, R., Liniger, M. A., & Appenzeller, C. (2010). Risks of model weighting in multimodel climate projections. *Journal of Climate*, *23*, 4175–4191. https://doi.org/10.1175/2010JCLI3594.1
54. Lanzante, J. R. (2021). Testing for differences between two distributions in the presence of serial correlation using the Kolmogorov–Smirnov and Kuiper's tests. *International Journal of Climatology*, *41*, 6314–6323. https://doi.org/10.1002/joc.7196
55. Menne, M. J., Durre, I., Vose, R. S., Gleason, B. E., & Houston, T. G. (2012). An overview of the global historical climatology network-daily database. *Journal of Atmospheric and Oceanic Technology*, *29*, 897–910. https://doi.org/10.1175/JTECH-D-11-00103.1
56. Koppe, C., Kovats, S., Jendritzky, G., & Menne, B. (2004). *Heat-waves: Risks and responses*. World Health Organization. Regional Office for Europe.
57. Steadman, R. G. (1979). The assessment of sultriness. Part I: A temperature-humidity index based on human physiology and clothing science. *Journal of Applied Meteorology and Climatology*, *18*, 861–873. https://doi.org/10.1175/1520-0450(1979)018⟨0861:TAOSPI⟩2.0.CO;2
58. Rothfusz, L. P. (1990). *The heat index 'equation' (or, more than you ever wanted to know about heat index)*. National Weather Service.
59. Lu, Y. C., & Romps, D. M. (2022). Extending the Heat Index. https://journals.ametsoc.org/view/journals/apme/61/10/JAMC-D-22-0021.1.xml
60. National Centers for Environmental Information (NCEI). (2023). U.S. Hourly Precipitation Data (HPD).
61. National Centers for Environmental Information (NCEI). (2023). U.S. Local Climatological Data (LCD).
62. Restrepo-Posada, P. J., & Eagleson, P. S. (1982). Identification of independent rainstorms. *Journal of Hydrology*, *55*, 303–319. https://doi.org/10.1016/0022-1694(82)90136-6
63. Yu, Z., Miller, S., Montalto, F., & Lall, U. (2018). The bridge between precipitation and temperature—Pressure Change Events: Modeling future non-stationary precipitation. *Journal of Hydrology*, *562*, 346–357. https://doi.org/10.1016/j.jhydrol.2018.05.014
64. Hussain, M., & Mahmud, I. (2019). pyMannKendall: A python package for non parametric Mann Kendall family of trend tests. *Journal of Open Source Software*, *4*, 1556. https://doi.org/10.21105/joss.01556
65. Milly, P. C. D., Betancourt, J., Falkenmark, M., Hirsch, R. M., Kundzewicz, Z. W., Lettenmaier, D. P., & Stouffer, R. J. (2008). Stationarity is dead: Whither water management? *Science*, *319*, 573–574. https://doi.org/10.1126/science.1151915
66. Allan, R. P., & Soden, B. J. (2008). Atmospheric warming and the amplification of precipitation extremes. *Science*, *321*, 1481–1484. https://doi.org/10.1126/science.1160787
67. Fowler, H. J., Lenderink, G., Prein, A. F., Westra, S., Allan, R. P., Ban, N., Barbero, R., Berg, P., Blenkinsop, S., Do, H. X., Guerreiro, S., Haerter, J. O., Kendon, E. J., Lewis, E., Schaer, C., Sharma, A., Villarini, G., Wasko, C., & Zhang, X. (2021). Anthropogenic intensification of short-duration rainfall extremes. *Nature Reviews Earth & Environment*, *2*, 107–122. https://doi.org/10.1038/s43017-020-00128-6
68. Pfahl, S., O'gorman, P. A., & Fischer, E. M. (2017). Understanding the regional pattern of projected future changes in extreme precipitation. *Nature Climate Change*, *7*, 423–427. https://doi.org/10.1038/nclimate3287
69. National Oceanic and Atmospheric Administration. (2022). *Weather, Water, and Climate Strategy: FY 2023–2027*. NOAA.
70. Perica, S., Pavlovic, S., Laurent, M. S., Trypaluk, C., Unruh, D., Martin, D., & Wilhite, O. (2019). *NOAA Atlas 14: Precipitation Frequency Atlas of the United States Volume 10 Version 3.0: Northeastern States*. National Weather Service.
71. Ditlevsen, P., & Ditlevsen, S. (2023). Warning of a forthcoming collapse of the Atlantic meridional overturning circulation. *Nature Communications*, *14*, 4254. https://doi.org/10.1038/s41467-023-39810-w
72. Liu, W., Fedorov, A. V., Xie, S. P., & Hu, S. (2020). Climate impacts of a weakened Atlantic Meridional Overturning Circulation in a warming climate. *Science Advances*, *6*, eaaz4876. https://doi.org/10.1126/sciadv.aaz4876
73. Krasting, J. P., Dunne, J. P., Stouffer, R. J., & Hallberg, R. W. (2016). Enhanced Atlantic sea-level rise relative to the Pacific under high carbon emission rates. *Nature Geoscience*, *9*, 210–214. https://doi.org/10.1038/ngeo2641
74. Yin, J., & Goddard, P. B. (2013). Oceanic control of sea level rise patterns along the East Coast of the United States: U.S. East Coast sea level rise. *Geophysical Research Letters*, *40*, 5514–5520. https://doi.org/10.1002/2013GL057992
75. Coumou, D., & Robinson, A. (2013). Historic and future increase in the global land area affected by monthly heat extremes. *Environmental Research Letters*, *8*, 034018. https://doi.org/10.1088/1748-9326/8/3/034018
76. Habeeb, D., Vargo, J., & Stone, B. (2015). Rising heat wave trends in large US cities. *Natural Hazards*, *76*, 1651–1665. https://doi.org/10.1007/s11069-014-1563-z
77. Horton, R. M., Mankin, J. S., Lesk, C., Coffel, E., & Raymond, C. (2016). A review of recent advances in research on extreme heat events. *Current Climate Change Reports*, *2*, 242–259. https://doi.org/10.1007/s40641-016-0042-x
78. Horton, D. E., Johnson, N. C., Singh, D., Swain, D. L., Rajaratnam, B., & Diffenbaugh, N. S. (2015). Contribution of changes in atmospheric circulation patterns to extreme temperature trends. *Nature*, *522*, 465–469. https://doi.org/10.1038/nature14550
79. Jeong, D. I., Cannon, A. J., & Yu, B. (2022). Influences of atmospheric blocking on North American summer heatwaves in a changing climate: A comparison of two Canadian Earth system model large ensembles. *Climatic Change*, *172*, 5. https://doi.org/10.1007/s10584-022-03358-3
80. Miralles, D. G., Teuling, A. J., Van Heerwaarden, C. C., & Vilà-Guerau De Arellano, J. (2014). Mega-heatwave temperatures due to combined soil desiccation and atmospheric heat accumulation. *Nature Geoscience*, *7*, 345–349. https://doi.org/10.1038/ngeo2141
81. Calvin, K., Dasgupta, D., Krinner, G., Mukherji, A., Thorne, P. W., Trisos, C., Romero, J., Aldunce, P., Barrett, K., Blanco, G., Cheung, W. W. L., Connors, S., Denton, F., Diongue-Niang, A., Dodman, D., Garschagen, M., Geden, O., Hayward, B., Jones, C., … Péan, C. (2023). *IPCC, 2023:*

Climate Change 2023: Synthesis Report. Contribution of Working Groups I, II and III to the Sixth Assessment Report of the Intergovernmental Panel on Climate Change [Core Writing Team, H. Lee and J. Romero (eds.)]. IPCC, Geneva, Switzerland. Intergovernmental Panel on Climate Change (IPCC). https://doi.org/10.59327/IPCC/AR6-9789291691647

82. Oke, T. R. (1982). The energetic basis of the urban heat island. *Quarterly Journal of the Royal Meteorological Society*, *108*, 1–24. https://doi.org/10.1002/qj.49710845502
83. Mallen, E., Bakin, J., Stone, B., Sivakumar, R., & Lanza, K. (2020). Thermal impacts of built and vegetated environments on local microclimates in an Urban University campus. *Urban Climate*, *32*, 100640. https://doi.org/10.1016/j.uclim.2020.100640
84. Mcconnell, K., Braneon, C. V., Glenn, E., Stamler, N., Mallen, E., Johnson, D. P., Pandya, R., Abramowitz, J., Fernandez, G., & Rosenzweig, C. (2022). A quasi-experimental approach for evaluating the heat mitigation effects of green roofs in Chicago, Illinois. *Sustainable Cities and Society*, *76*, 103376. https://doi.org/10.1016/j.scs.2021.103376
85. Memon, R. A., Leung, D. Y. C., & Liu, C. H. (2009). An investigation of urban heat island intensity (UHII) as an indicator of urban heating. *Atmospheric Research*, *94*, 491–500. https://doi.org/10.1016/j.atmosres.2009.07.006
86. Almeida, C. R. D., Teodoro, A. C., & Gonçalves, A. (2021). Study of the urban heat island (UHI) using remote sensing data/techniques: A systematic review. *Environments*, *8*, 105. https://doi.org/10.3390/environments8100105
87. Wang, Z. H. (2022). Reconceptualizing urban heat island: Beyond the urban-rural dichotomy. *Sustainable Cities and Society*, *77*, 103581. https://doi.org/10.1016/j.scs.2021.103581
88. Cai, X., Yang, J., Zhang, Y., Xiao, X., & Xia, J. (2023). Cooling island effect in urban parks from the perspective of internal park landscape. *Humanities and Social Sciences Communications*, *10*, 674. https://doi.org/10.1057/s41599-023-02209-5
89. Yao, X., Yu, K., Zeng, X., Lin, Y., Ye, B., Shen, X., & Liu, J. (2022). How can urban parks be planned to mitigate urban heat island effect in "Furnace cities"? An accumulation perspective. *Journal of Cleaner Production*, *330*, 129852. https://doi.org/10.1016/j.jclepro.2021.129852
90. Gough, W. A., & Leung, A. C. W. (2022). Do airports have their own climate? *Meteorology*, *1*, 171–182. https://doi.org/10.3390/meteorology1020012
91. Wan, J., Yong, B., & Zhou, X. (2022). Spatial and temporal analysis of the increasing effects of large-scale infrastructure construction on the surface urban heat island. *Ecotoxicology and Environmental Safety*, *237*, 113521. https://doi.org/10.1016/j.ecoenv.2022.113521
92. Zhou, X., Okaze, T., Ren, C., Cai, M., Ishida, Y., Watanabe, H., & Mochida, A. (2020). Evaluation of urban heat islands using local climate zones and the influence of sea-land breeze. *Sustainable Cities and Society*, *55*, 102060. https://doi.org/10.1016/j.scs.2020.102060
93. Hamstead, Z. A., Kremer, P., Larondelle, N., Mcphearson, T., & Haase, D. (2016). Classification of the heterogeneous structure of urban landscapes (STURLA) as an indicator of landscape function applied to surface temperature in New York City. *Ecological Indicators*, *70*, 574–585. https://doi.org/10.1016/j.ecolind.2015.10.014
94. Broadbent, A. M., Declet-Barreto, J., Krayenhoff, E. S., Harlan, S. L., & Georgescu, M. (2022). Targeted implementation of cool roofs for equitable urban adaptation to extreme heat. *Science of the Total Environment*, *811*, 151326. https://doi.org/10.1016/j.scitotenv.2021.151326
95. Heger, M. (2022). Equitable adaptation to extreme heat impacts of climate change. *Journal of Environmental Law and Policy*, *39*, 283–312. https://doi.org/10.5070/L539256965
96. Shi, R., Hobbs, B. F., Quinn, J. D., Lempert, R., & Knopman, D. (2023). City-Heat Equity Adaptation Tool (City-HEAT): Multi-objective optimization of environmental modifications and human heat exposure reductions for urban heat adaptation under uncertainty. *Environmental Modelling & Software*, *160*, 105607. https://doi.org/10.1016/j.envsoft.2022.105607
97. Bornstein, R. D. (1968). Observations of the urban heat island effect in New York City. *Journal of Applied Meteorology and Climatology*, *7*, 575–582. https://doi.org/10.1175/1520-0450(1968)007⟨0575:OOTUHI⟩2.0.CO;2
98. Gedzelman, S. D., Austin, S., Cermak, R., Stefano, N., Partridge, S., Quesenberry, S., & Robinson, D. A. (2003). Mesoscale aspects of the urban heat island around New York City. *Theoretical and Applied Climatology*, *75*, 29–42. https://doi.org/10.1007/s00704-002-0724-2
99. Raven, J., Braneon, C., & Rosenzweig, C. (2022). Embedding climate change in urban planning and urban design in New York City. In C. Ren, & G. McGregor (Eds.), *Urban climate science for planning healthy cities* (pp. 45–70). Springer International Publishing. https://doi.org/10.1007/978-3-030-87598-5
100. Bauer, T. J. (2020). Interaction of urban heat island effects and land–sea breezes during a New York City heat event. *Journal of Applied Meteorology and Climatology*, *59*, 477–495. https://doi.org/10.1175/JAMC-D-19-0061.1
101. Ortiz, L. E., Gonzalez, J. E., Wu, W., Schoonen, M., Tongue, J., & Bornstein, R. (2018). New York City impacts on a regional heat wave. *Journal of Applied Meteorology and Climatology*, *57*, 837–851. https://doi.org/10.1175/JAMC-D-17-0125.1
102. Alonzo, M., Baker, M. E., Gao, Y., & Shandas, V. (2021). Spatial configuration and time of day impact the magnitude of urban tree canopy cooling. *Environmental Research Letters*, *16*, 084028. https://doi.org/10.1088/1748-9326/ac12f2
103. Shiflett, S. A., Liang, L. L., Crum, S. M., Feyisa, G. L., Wang, J., & Jenerette, G. D. (2017). Variation in the urban vegetation, surface temperature, air temperature nexus. *Science of the Total Environment*, *579*, 495–505. https://doi.org/10.1016/j.scitotenv.2016.11.069
104. Zekar, A., Milojevic-Dupont, N., Zumwald, M., Wagner, F., & Creutzig, F. (2023). Urban form features determine spatio-temporal variation of ambient temperature: A comparative study of three European cities. *Urban Climate*, *49*, 101467. https://doi.org/10.1016/j.uclim.2023.101467
105. Ziter, C. D., Pedersen, E. J., Kucharik, C. J., & Turner, M. G. (2019). Scale-dependent interactions between tree canopy cover and impervious surfaces reduce daytime urban heat during summer. *Proceedings of the National Academy of Sciences*, *116*, 7575–7580. https://doi.org/10.1073/pnas.1817561116
106. Chen, Y., Wu, J., Yu, K., & Wang, D. (2020). Evaluating the impact of the building density and height on the block surface temperature. *Building and Environment*, *168*, 106493. https://doi.org/10.1016/j.buildenv.2019.106493
107. Konarska, J., Holmer, B., Lindberg, F., & Thorsson, S. (2016). Influence of vegetation and building geometry on the spatial variations of air temperature and cooling rates in a high-latitude city. *International Journal of Climatology*, *36*, 2379–2395. https://doi.org/10.1002/joc.4502
108. Johnson, S., Ross, Z., Kheirbek, I., & Ito, K. (2020). Characterization of intra-urban spatial variation in observed summer ambient temperature from the New York City Community Air Survey. *Urban Climate*, *31*, 100583. https://doi.org/10.1016/j.uclim.2020.100583
109. City of New York Mayor's Office of Resiliency. (2017). *Cool Neighborhoods NYC: A comprehensive approach to keep communities safe in extreme heat*. City of New York Mayor's Office of Resiliency.
110. City of New York Department of Health and Mental Hygiene. (2023). NYC DOH Environment and Health Data Portal. https://a816-dohbesp.nyc.gov/IndicatorPublic/beta/key-topics/climatehealth/heat-report/
111. Li, D., & Bou-Zeid, E. (2013). Synergistic interactions between urban heat islands and heat waves: The impact in cities is larger than the

sum of its parts. *Journal of Applied Meteorology and Climatology*, *52*, 2051–2064. https://doi.org/10.1175/JAMC-D-13-02.1
112. Ramamurthy, P., González, J., Ortiz, L., Arend, M., & Moshary, F. (2017). Impact of heatwave on a megacity: An observational analysis of New York City during July 2016. *Environmental Research Letters*, *12*, 054011. https://doi.org/10.1088/1748-9326/aa6e59
113. Quiggin, J. (2018). The importance of 'extremely unlikely' events: Tail risk and the costs of climate change. *Australian Journal of Agricultural and Resource Economics*, *62*, 4–20. https://doi.org/10.1111/1467-8489.12238
114. Orton, P. M., Hall, T. M., Talke, S. A., Blumberg, A. F., Georgas, N., & Vinogradov, S. (2016). A validated tropical-extratropical flood hazard assessment for New York Harbor. *Journal of Geophysical Research, Oceans*, *121*, 8904–8929. https://doi.org/10.1002/2016JC011679
115. Federal Emergency Management Agency. (2007). *Flood Insurance Study, City of New York, NY (All Jurisdictions)*. U.S. Federal Emergency Management Agency.
116. Sweet, W., Zervas, C., Gill, S., & Park, J. (2013). 6. Hurricane Sandy inundation probabilities today and tomorrow. In T. C. Peterson, M. P. Hoerling, P. A. Stott, & S. C. Herring (Eds.), *Explaining extreme events of 2012 from a climate perspective* (pp. S13–S20). American Meteorological Society.
117. Trenberth, K. E., Dai, A., Rasmussen, R. M., & Parsons, D. B. (2003). The changing character of precipitation. *Bulletin of the American Meteorological Society*, *84*, 1205–1218. https://doi.org/10.1175/BAMS-84-9-1205
118. Lenderink, G., Barbero, R., Loriaux, J. M., & Fowler, H. J. (2017). Super-Clausius–Clapeyron scaling of extreme hourly convective precipitation and its relation to large-scale atmospheric conditions. *Journal of Climate*, *30*, 6037–6052. https://doi.org/10.1175/JCLI-D-16-0808.1
119. Loriaux, J. M., Lenderink, G., & Siebesma, A. P. (2017). Large-scale controls on extreme precipitation. *Journal of Climate*, *30*, 955–968. https://doi.org/10.1175/JCLI-D-16-0381.1
120. Santer, B. D., Wehner, M. F., Wigley, T. M. L., Sausen, R., Meehl, G. A., Taylor, K. E., Ammann, C., Arblaster, J., Washington, W. M., Boyle, J. S., & BrüGgemann, W. (2003). Contributions of anthropogenic and natural forcing to recent tropopause height changes. *Science*, *301*, 479–483. https://doi.org/10.1126/science.1084123
121. Teale, N., & Robinson, D. A. (2020). Patterns of water vapor transport in the eastern United States. *Journal of Hydrometeorology*, *21*, 2123–2138. https://doi.org/10.1175/JHM-D-19-0267.1
122. Barlow, M. (2011). Influence of hurricane-related activity on North American extreme precipitation: Hurricanes and North American extremes. *Geophysical Research Letters*, *38*, 1–5. https://doi.org/10.1029/2010GL046258
123. National Oceanic and Atmospheric Administration. (2023). *Service Assessment: August–September 2021 Hurricane Ida*. NOAA SPD.
124. Moseley, C., Hohenegger, C., Berg, P., & Haerter, J. O. (2016). Intensification of convective extremes driven by cloud–cloud interaction. *Nature Geoscience*, *9*, 748–752. https://doi.org/10.1038/ngeo2789
125. Jessup, S. M., & Colucci, S. J. (2012). Organization of flash-flood-producing precipitation in the northeast United States. *Weather and Forecasting*, *27*, 345–361. https://doi.org/10.1175/WAF-D-11-00026.1
126. Pendergrass, A. G. (2020). Changing degree of convective organization as a mechanism for dynamic changes in extreme precipitation. *Current Climate Change Reports*, *6*, 47–54. https://doi.org/10.1007/s40641-020-00157-9
127. Lochbihler, K., Lenderink, G., & Siebesma, A. P. (2019). Response of extreme precipitating cell structures to atmospheric warming. *JGR Atmospheres*, *124*, 6904–6918. https://doi.org/10.1029/2018JD029954
128. Prein, A. F., Liu, C., Ikeda, K., Trier, S. B., Rasmussen, R. M., Holland, G. J., & Clark, M. P. (2017). Increased rainfall volume from future convective storms in the US. *Nature Climate Change*, *7*, 880–884. https://doi.org/10.1038/s41558-017-0007-7
129. Singh, M. S., & O'gorman, P. A. (2015). Increases in moist-convective updraught velocities with warming in radiative-convective equilibrium. *Quarterly Journal of the Royal Meteorological Society*, *141*, 2828–2838. https://doi.org/10.1002/qj.2567
130. Bao, J., & Sherwood, S. C. (2019). The role of convective self-aggregation in extreme instantaneous versus daily precipitation. *Journal of Advances in Modeling Earth Systems*, *11*, 19–33. https://doi.org/10.1029/2018MS001503
131. Parodi, A., & Emanuel, K. (2009). A theory for buoyancy and velocity scales in deep moist convection. *Journal of the Atmospheric Sciences*, *66*, 3449–3463. https://doi.org/10.1175/2009JAS3103.1
132. Naughten, K. A., Holland, P. R., & De Rydt, J. (2023). Unavoidable future increase in West Antarctic ice-shelf melting over the twenty-first century. *Nature Climate Change*, *13*, 1222–1228. https://doi.org/10.1038/s41558-023-01818-x
133. Bochow, N., Poltronieri, A., Robinson, A., Montoya, M., Rypdal, M., & Boers, N. (2023). Overshooting the critical threshold for the Greenland ice sheet. *Nature*, *622*, 528–536. https://doi.org/10.1038/s41586-023-06503-9
134. Gori, A., Lin, N., Xi, D., & Emanuel, K. (2022). Tropical cyclone climatology change greatly exacerbates US extreme rainfall–surge hazard. *Nature Climate Change*, *12*, 171–178. https://doi.org/10.1038/s41558-021-01272-7
135. Cialone, M. A., Massey, T. C., Anderson, M. E., Grzegorzewski, A. S., Jensen, R. E., Cialone, A., Mark, D. J., Pevey, K. C., Gunkel, B. L., McAlpin, T. O., Nadal-Caraballo, N. C., Melby, J. A., & Ratcliff, J. J. (2015). *North Atlantic Coast Comprehensive Study (NACCS) Coastal Storm Model Simulations: Waves and Water Levels*. U.S. Army Corps of Engineers. Engineer Research and Development Center.
136. Federal Emergency Management Agency. (2014). *Region II Coastal Storm Surge Study: Overview*. FEMA.
137. McPhearson, T., Towers, J., Balk, D., Horton, R., Madajewicz, M., Montalto, F., Neidell, M., Orton, P. M., Rosenzweig, B., Bader, D., Chen, Z., DeGaetano, A., Evans, C., Golkhandan, M. R., Gurian, P., Kaatz, J., Herreros-Cantis, P., Lo, R., Ortiz, L., … Zoraghein, H. (2024). *New York City Town+Gown Climate Vulnerability, Impact, and Adaptation (VIA) Analysis: Final Report*. City of New York Mayor's Office of Climate and Environmental Justice.
138. Lin, N., Emanuel, K., Oppenheimer, M., & Vanmarcke, E. (2012). Physically based assessment of hurricane surge threat under climate change. *Nature Climate Change*, *2*, 462–467. https://doi.org/10.1038/nclimate1389
139. Dullaart, J. C. M., Muis, S., Bloemendaal, N., Chertova, M. V., Couasnon, A., & Aerts, J. C. J. H. (2021). Accounting for tropical cyclones more than doubles the global population exposed to low-probability coastal flooding. *Communications Earth & Environment*, *2*, 135. https://doi.org/10.1038/s43247-021-00204-9
140. National Oceanic and Atmospheric Administration. (2023). NOAA Tides & Currents. https://tidesandcurrents.noaa.gov/est/
141. Degaetano, A. T., & Castellano, C. M. (2017). Future projections of extreme precipitation intensity-duration-frequency curves for climate adaptation planning in New York State. *Climate Services*, *5*, 23–35. https://doi.org/10.1016/j.cliser.2017.03.003
142. Kunkel, K. E., Stevens, S. E., Stevens, L. E., & Karl, T. R. (2020). Observed climatological relationships of extreme daily precipitation events with precipitable water and vertical velocity in the contiguous United States. *Geophysical Research Letters*, *47*, e2019GL086721. https://doi.org/10.1029/2019GL086721
143. Miro, M. E., DeGaetano, A. T., López-Cantú, T., Samaras, C., Webber, M., & Grocholski, K. R. (2021). *Developing future projected intensity-duration-frequency (IDF) curves: A technical report on data, methods,*

and IDF curves for the Chesapeake Bay Watershed and Virginia. RAND Corporation. https://doi.org/10.7249/TLA1365-1

144. National Weather Service. (2022). *Analysis of Impact on Nonstationary Climate on NOAA Atlas 14 Estimates: Assessment Report*. National Oceanic and Atmospheric Administration.
145. Cannon, A. J., Sobie, S. R., & Murdock, T. Q. (2015). Bias correction of GCM precipitation by quantile mapping: How well do methods preserve changes in quantiles and extremes? *Journal of Climate*, *28*, 6938–6959. https://doi.org/10.1175/JCLI-D-14-00754.1
146. Pierce, D. W., Cayan, D. R., & Thrasher, B. L. (2014). Statistical downscaling using Localized Constructed Analogs (LOCA)*. *Journal of Hydrometeorology*, *15*, 2558–2585. https://doi.org/10.1175/JHM-D-14-0082.1
147. Pierce, D. W., Cayan, D. R., Feldman, D. R., & Risser, M. D. (2023). Future increases in North American extreme precipitation in CMIP6 downscaled with LOCA. *Journal of Hydrometeorology*, *24*, 951–975. https://doi.org/10.1175/JHM-D-22-0194.1
148. Livneh, B., Bohn, T. J., Pierce, D. W., Munoz-Arriola, F., Nijssen, B., Vose, R., Cayan, D. R., & Brekke, L. (2015). A spatially comprehensive, hydrometeorological data set for Mexico, the U.S., and Southern Canada 1950–2013. *Scientific Data*, *2*, 150042. https://doi.org/10.1038/sdata.2015.42
149. Pierce, D. W., Su, L., Cayan, D. R., Risser, M. D., Livneh, B., & Lettenmaier, D. P. (2021). An Extreme-Preserving Long-Term Gridded Daily Precipitation Dataset for the Conterminous United States. https://journals.ametsoc.org/view/journals/hydr/22/7/JHM-D-20-0212.1.xml
150. Maimone, M., Malter, S., Anbessie, T., & Rockwell, J. (2023). Three methods of characterizing climate-induced changes in extreme rainfall: A comparison study. *Journal of Water and Climate Change*, *14*, 4245–4260. https://doi.org/10.2166/wcc.2023.420
151. Maimone, M., Malter, S., Rockwell, J., & Raj, V. (2019). Transforming global climate model precipitation output for use in urban stormwater applications. *Journal of Water Resources Planning and Management*, *145*, 04019021. https://doi.org/10.1061/(ASCE)WR.1943-5452.0001071
152. Kendon, E. J., Ban, N., Roberts, N. M., Fowler, H. J., Roberts, M. J., Chan, S. C., Evans, J. P., Fosser, G., & Wilkinson, J. M. (2017). Do convection-permitting regional climate models improve projections of future precipitation change? *Bulletin of the American Meteorological Society*, *98*, 79–93. https://doi.org/10.1175/BAMS-D-15-0004.1
153. Luo, P., Luo, M., Li, F., Qi, X., Huo, A., Wang, Z., He, B., Takara, K., Nover, D., & Wang, Y. (2022). Urban flood numerical simulation: Research, methods and future perspectives. *Environmental Modelling & Software*, *156*, 105478. https://doi.org/10.1016/j.envsoft.2022.105478
154. Luong, T. M., Dasari, H. P., & Hoteit, I. (2020). Impact of urbanization on the simulation of extreme rainfall in the City of Jeddah, Saudi Arabia. *Journal of Applied Meteorology and Climatology*, *59*, 953–971. https://doi.org/10.1175/JAMC-D-19-0257.1
155. Ban, N., Caillaud, C., Coppola, E., Pichelli, E., Sobolowski, S., Adinolfi, M., Ahrens, B., Alias, A., Anders, I., Bastin, S., Belušić, D., Berthou, S., Brisson, E., Cardoso, R. M., Chan, S. C., Christensen, O. B., Fernández, J., Fita, L., Frisius, T., … Zander, M. J. (2021). The first multi-model ensemble of regional climate simulations at kilometer-scale resolution, part I: Evaluation of precipitation. *Climate Dynamics*, *57*, 275–302. https://doi.org/10.1007/s00382-021-05708-w
156. Pichelli, E., Coppola, E., Sobolowski, S., Ban, N., Giorgi, F., Stocchi, P., Alias, A., Belušić, D., Berthou, S., Caillaud, C., Cardoso, R. M., Chan, S., Christensen, O. B., Dobler, A., De Vries, H., Goergen, K., Kendon, E. J., Keuler, K., Lenderink, G., … Vergara-Temprado, J. (2021). The first multi-model ensemble of regional climate simulations at kilometer-scale resolution part 2: Historical and future simulations of precipitation. *Climate Dynamics*, *56*, 3581–3602. https://doi.org/10.1007/s00382-021-05657-4
157. Kendon, E. J., Prein, A. F., Senior, C. A., & Stirling, A. (2021). Challenges and outlook for convection-permitting climate modelling. *Philosophical Transactions of the Royal Society A*, *379*, 20190547. https://doi.org/10.1098/rsta.2019.0547
158. Matte, T. D., Lane, K., Tipaldo, J., Barnes, J., Knowlton, K., Torem, E., Anand, G., Yoon, L., Marcotullio, P., Balk, D., Constible, J., Elszasz, H., Ito, K., Jessel, S., Limaye, V., Parks, R., Rutigliano, M., Sorenson, C., & Yuan, A. (2024). NPCC4: Climate change and New York City's health risk. Annals of New York Academy of Sciences, 1–56.
159. Chakraborty, T., Hsu, A., Manya, D., & Sheriff, G. (2019). Disproportionately higher exposure to urban heat in lower-income neighborhoods: A multi-city perspective. *Environmental Research Letters*, *14*, 105003. https://doi.org/10.1088/1748-9326/ab3b99
160. Wilson, B. (2020). Urban heat management and the legacy of redlining. *Journal of the American Planning Association*, *86*, 443–457. https://doi.org/10.1080/01944363.2020.1759127
161. Burls, N., & Sagoo, N. (2022). Increasingly sophisticated climate models need the out-of-sample tests paleoclimates provide. *Journal of Advances in Modeling Earth Systems*, *14*, e2022MS003389. https://doi.org/10.1029/2022MS003389
162. Masson-Delmotte, V., Zhai, P., Pirani, A., Connors, S. L., Péan, C., Chen, Y., Goldfarb, L., Gomis, M. I., Matthews, J. B. R., Berger, S., Huang, M., Yelekçi, O., Yu, R., Zhou, B., Lonnoy, E., Maycock, T. K., Waterfield, T., Leitzell, K., & Caud, N. (Eds.) (2021). *Climate Change 2021 – The Physical Science Basis: Working Group I Contribution to the Sixth Assessment Report of the Intergovernmental Panel on Climate Change* (1st ed.). Cambridge University Press. https://doi.org/10.1017/9781009157896
163. Zhu, J., Poulsen, C. J., & Otto-Bliesner, B. L. (2020). High climate sensitivity in CMIP6 model not supported by paleoclimate. *Nature Climate Change*, *10*, 378–379. https://doi.org/10.1038/s41558-020-0764-6
164. Milillo, P., Rignot, E., Rizzoli, P., Scheuchl, B., Mouginot, J., Bueso-Bello, J. L., Prats-Iraola, P., & Dini, L. (2022). Rapid glacier retreat rates observed in West Antarctica. *Nature Geoscience*, *15*, 48–53. https://doi.org/10.1038/s41561-021-00877-z
165. Morlighem, M., Rignot, E., Binder, T., Blankenship, D., Drews, R., Eagles, G., Eisen, O., Ferraccioli, F., Forsberg, R., Fretwell, P., Goel, V., Greenbaum, J. S., Gudmundsson, H., Guo, J., Helm, V., Hofstede, C., Howat, I., Humbert, A., Jokat, W., … Young, D. A. (2020). Deep glacial troughs and stabilizing ridges unveiled beneath the margins of the Antarctic ice sheet. *Nature Geoscience*, *13*, 132–137. https://doi.org/10.1038/s41561-019-0510-8
166. Wild, C. T., Alley, K. E., Muto, A., Truffer, M., Scambos, T. A., & Pettit, E. C. (2022). Weakening of the pinning point buttressing Thwaites Glacier, West Antarctica. *Cryosphere*, *16*, 397–417. https://doi.org/10.5194/tc-16-397-2022
167. Schmidt, B. E., Washam, P., Davis, P. E. D., Nicholls, K. W., Holland, D. M., Lawrence, J. D., Riverman, K. L., Smith, J. A., Spears, A., Dichek, D. J. G., Mullen, A. D., Clyne, E., Yeager, B., Anker, P., Meister, M. R., Hurwitz, B. C., Quartini, E. S., Bryson, F. E., Basinski-Ferris, A., … Makinson, K. (2023). Heterogeneous melting near the Thwaites Glacier grounding line. *Nature*, *614*, 471–478. https://doi.org/10.1038/s41586-022-05691-0
168. Barletta, V. R., Bevis, M., Smith, B. E., Wilson, T., Brown, A., Bordoni, A., Willis, M., Khan, S. A., Rovira-Navarro, M., Dalziel, I., Smalley, R., Kendrick, E., Konfal, S., Caccamise, D. J., Aster, R. C., Nyblade, A., & Wiens, D. A. (2018). Observed rapid bedrock uplift in Amundsen Sea Embayment promotes ice-sheet stability. *Science*, *360*, 1335–1339. https://doi.org/10.1126/science.aao1447
169. Gomez, N., Pollard, D., & Holland, D. (2015). Sea-level feedback lowers projections of future Antarctic Ice-Sheet mass loss. *Nature Communications*, *6*, 8798. https://doi.org/10.1038/ncomms9798

170. Clerc, F., Minchew, B. M., & Behn, M. D. (2019). Marine ice cliff instability mitigated by slow removal of ice shelves. *Geophysical Research Letters*, *46*, 12108–12116. https://doi.org/10.1029/2019GL084183
171. Robel, A. A., & Banwell, A. F. (2019). A speed limit on ice shelf collapse through hydrofracture. *Geophysical Research Letters*, *46*, 12092–12100. https://doi.org/10.1029/2019GL084397
172. Edwards, T. L., Brandon, M. A., Durand, G., Edwards, N. R., Golledge, N. R., Holden, P. B., Nias, I. J., Payne, A. J., Ritz, C., & Wernecke, A. (2019). Revisiting Antarctic ice loss due to marine ice-cliff instability. *Nature*, *566*, 58–64. https://doi.org/10.1038/s41586-019-0901-4
173. Childs, P. P., & Raman, S. (2005). Observations and numerical simulations of urban heat island and sea breeze circulations over New York City. *Pure and Applied Geophysics*, *162*, 1955–1980. https://doi.org/10.1007/s00024-005-2700-0
174. Scott, A. A., Waugh, D. W., & Zaitchik, B. F. (2018). Reduced Urban Heat Island intensity under warmer conditions. *Environmental Research Letters*, *13*, 064003. https://doi.org/10.1088/1748-9326/aabd6c

How to cite this article: Ortiz, L., Braneon, C., Horton, R., Bader, D., Orton, P., Gornitz, V., Rosenzweig, B., McPhearson, T., Smalls-Mantey, L., Sheerazi, H., Montalto, F. A., Golkhandan, M. R., Evans, C., DeGaetano, A., Mallen, E., Carter, L., McConnell, K., Mayo, T., & Buchanan, M. (2024). NPCC4: Tail risk, climate drivers of extreme heat, and new methods for extreme event projections. *Ann NY Acad Sci*., 1–28. https://doi.org/10.1111/nyas.15180

APPENDIX A: COMPARISON OF GCM ENSEMBLES

Boxplots comparing 960-member ensembles of annual projections with 780-member ensembles that exclude GCMs with TCR values greater than 2.2°C.

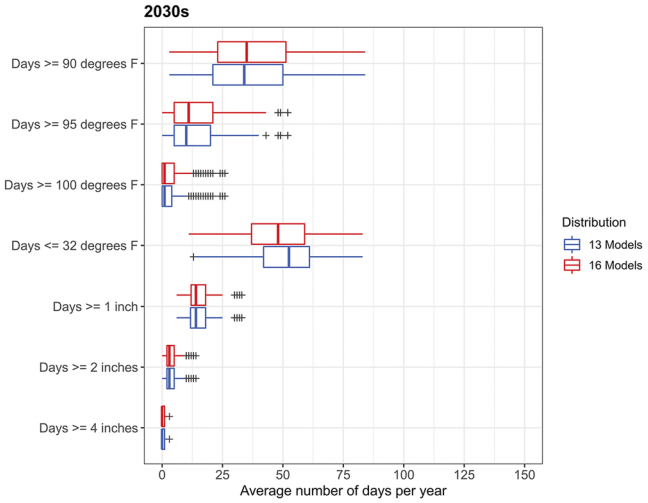

FIGURE A1 Boxplots comparing the 960-member ensemble (16 GCMs × 2 scenarios × 30 years) of annual projections for 2021–2050 with a 780-member ensemble (13 GCMs × 2 scenarios × 30 years) that excludes GCMs with TCR values greater than 2.2°C.

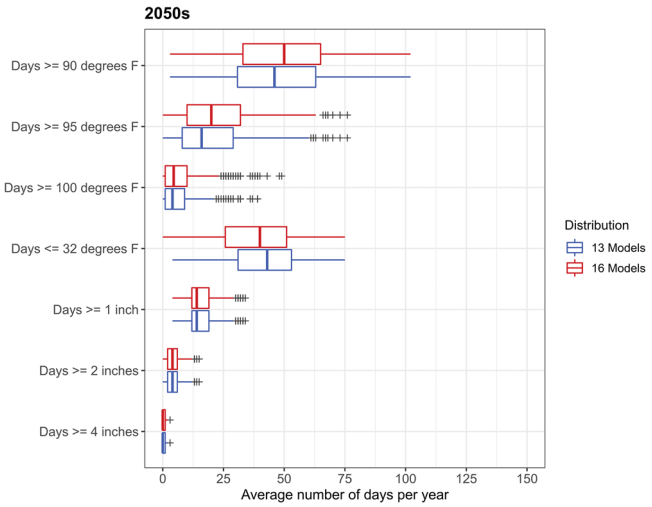

FIGURE A2 Boxplots comparing the 960-member ensemble (16 GCMs × 2 scenarios × 30 years) of annual projections for 2041–2070 with a 780-member ensemble (13 GCMs × 2 scenarios × 30 years) that excludes GCMs with TCR values greater than 2.2°C.

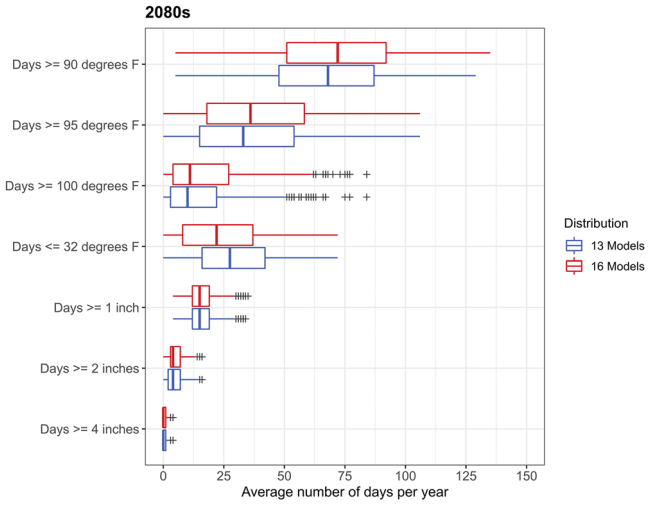

FIGURE A3 Boxplots comparing the 960-member ensemble (16 GCMs × 2 scenarios × 30 years) of annual projections for 2071–2100 with a 780-member ensemble (13 GCMs × 2 scenarios × 30 years) that excludes GCMs with TCR values greater than 2.2°C.